Department of Physics and Astronomy
University of Heidelberg

Master thesis

in Physics

submitted by

(name and surname)

born in (place of birth)

(year of submission)

Simulating effective field theories

on a space-time lattice with coloured noise

This Master thesis has been carried out by Matteo Zortea

at the

Institute for Theoretical Physics in Heidelberg

under the supervision of

Prof. Jan M. Pawloski

and

Dr. Felipe Attanasio

(Titel in Deutsch): (Abstract in Deutsch, max. 200 Worte)

(Title in English): (abstract in english, at most 200 words)

Erklärung:

Ich versichere, dass ich diese Arbeit selbstständig verfasst habe und keine anderen als die angegebenen Quellen und Hilfsmittel benutzt habe.

Heidelberg, den 27.11.2023 .....

Contents

List of Figures

List of Tables

"Grazie a tutti."

Matteo Zortea

Chapter 1

Introduction and outline

1.1 Quantum chromodynamics and its and phase diagram

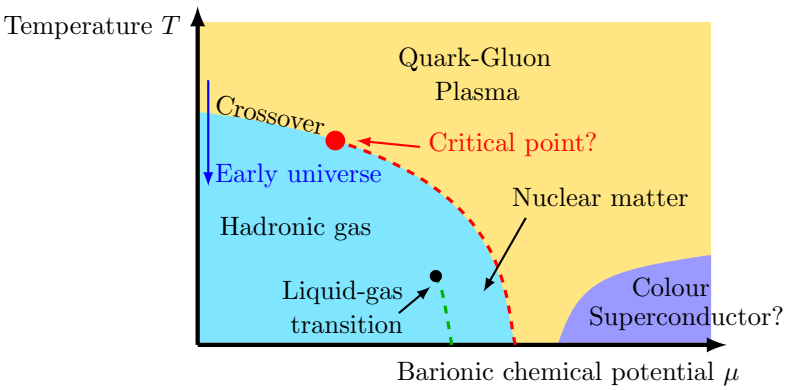

FIGURE 1.1

The phase diagram of Quantum Chromodynamics (QCD) stands as a captivating yet challenging terrain, encapsulating the diverse phases of matter under varying conditions of temperature and baryon density. At the heart of this diagram lies the intricate interplay between hadronic matter, characterized by the confinement of quarks and gluons within protons and neutrons, and the elusive quark-gluon plasma, a state believed to have existed microseconds after the Big Bang. Bridging these extremes are regions of phase transitions and critical points, where subtle changes in the system lead to transformative alterations in its properties. Investigating the QCD phase diagram is a formidable task, primarily due to the nonperturbative nature of the strong force. Analytical methods, often successful in perturbative regimes, falter in the face of the intense interactions among quarks and gluons at lower energy scales. This necessitates the use of numerical techniques, with lattice QCD simulations being a prominent approach. However, the lattice discretization introduces its own set of challenges, such as finite volume effects and the need for extrapolations to the continuum limit, adding layers of complexity to the study. Moreover, the precise determination of the location and nature of the critical point remains an unresolved puzzle, requiring sophisticated tools and innovative methodologies. Theoretical predictions must be juxtaposed with experimental observations, further complicating the quest for a comprehensive understanding of the QCD phase diagram.

1.2 The emergence of effective theories

A central role in our investigation will be played by the Wilsonian perspective of the Renormalization Group (RG). Within this paradigm, renormalization ceases to be merely a tool for taming divergences; the Wilsonian RG approach provides a way to resolve physics at different scales. The Wilson framework naturally brings to the concept of effective theory, a model which describes phenomena only in terms of relevant degrees of freedom. In the context of QCD, a diverse array of effective theories are introduce, tailored to specific aspects of the strong force dynamics. Some examples are the Quark Meson Model provides a framework for studying the interplay between quarks and mesons, shedding light on the transition between confined and deconfined phases. The Nambu-Jona-Lasinio model, explores the dynamical breaking of chiral symmetry and its consequences for hadron masses. This effective theory, rooted in the spontaneous symmetry breaking mechanism, offers valuable insights into the behavior of quarks and gluons in the low-energy regime. Another notable effective theory, the Gross-Neveu model, delves into the dynamics of massless fermions and their interactions, exhibiting chiral symmetry breaking and providing a simplified yet insightful perspective on certain aspects of QCD. The Gross-Neveu model, initially conceived in the realm of particle physics, finds surprising applications in condensed matter physics. Notably, it has been instrumental in the study of BCS superconductivity theory. The Gross-Neveu model's insights into the dynamics of massless fermions and its ability to describe chiral symmetry breaking have proven to be valuable in understanding the emergence of superconducting states in certain condensed matter systems.

1.3 Lattice Field Theory

Computing physical quantities from first principle approaches, is not only hard to do, but results often impossible due to the appearence of divergences in the calculations. To fix this, one often relies on expansion techniques such as perturbation theory (CITATION), in which one tries to regularise the theory order by order in an expansion on the interaction coupling, yielding finite quantities that depend on the truncation order. While this method is capable of producing incredibly precise results (g-2, fine structure, ...), it fails completely in treating non-perturbative phenomena, namely effects that cannot be captured by any order in the expansion or that are typical of strongly interacting systems. Example of such systems range from QCD, cold atoms, plasma, stuff. Moreover, such formulation is also not much suitable for numerical computations, since both the path integral and action measure are infinite dimensional objects.
Lattice field theory [1–4] is meant at first as a powerful non-perturbative regularisation tool to prevent divergences to occur and render the computation of the correlation functions finite. Moreover, it also provides a framework to study quantum field theory numerically on a computer. In order to accomplish this, one typically defines the theory on a spacetime lattice and makes use of statistical methods such as Monte Carlo algorithms to compute observables. One may wonder how can one reconstruct the results in the continuum theory, keeping the results finite, and matching the results on the discretised theory to physically measured ones. This task, far from beeing simple, will be the focus of the next sections, in which we will first introduce relevant theoretical tools, such as the renormalisation group, and then discuss

the existence of a continuum limit of a lattice theory and, if it exists, how it can be extracted. This will motivate the introduction of coloured noise in the context of continuum limits of effective theories, a technique which will be shown to be powerful also for other various reasons, which will be the main focus of the analysis carried in the remaining chapters.
We want to mention that the Yukawa theory (2.16) includes, as a special case, the Gross-Neveu model citation, which in turn is the 1+1 dimensional version of the Nambu-Jona-Lasinio model [5, 6]. More precisely, after dynamical bosonisation via a Hubbard-Stratonovich transformation either cite or show, the latter theories reduce to a Yukawa model with

$$K(x,y) = m_\phi^2\,\delta(x,y) \qquad \lambda = 0.$$

Da qualche parte cita [7]

1.4 Outline

Chapter 2 will be devoted to the introduction of the theoretical background that supports this work. We will start with the Kadanoff and Wilson approach to renormalisation in statistical physics and quantum field theory. Lattice field theory will then be introduced as a powerfool tool to simulate quantum field theory numerically and the basics of the formulation will be provided. We then turn to stochastic quantisation, the relation between noise and quantum fluctuations and how the standard formulation is modified by the presence of coloured noise. This will results in a deep connection between coloured stochastic quantisation and the renormalisation group. The chapter will end with a description of the model on which the above techniques are applied, namely a Yukawa theory.

Chapter 3 is devoted to detail techniques and methodologies of the project. We will start by explaining how the continuum model is discretised on a space-time lattice and how it can be simulated via a Monte Carlo method and stochastic quantisation. We will then list some possible applications of coloured noise in lattice QFT and describe some of the numerical experiments that will be carried in the last chapter.
The chapter will end with a description of the relevant observables that are employed to study a lattice quantum field theory.

Chapters 4 and 5 are devoted to the numerical investigation.
First, some premilinary analysis will be carried. We will show how fermionic masses are measured in the simulation and provide a panoramic over the general phase structure of the theory. The latter will guide the choice of parameter settings for all the simulations.
It will then be showed how coloured noise can be used to provide a smooth interpolation between the fully classical and fully quantum picture.
The introduction of noise can cause qualitative change in the behaviour of the system. In particular, it will be shown how quantum fluctuations can trigger a chiral phase transition in the model.
Finally we will show how coloured noise in combinations with the Kadanoff-Wilson RG can be used to cool a simulation by systematically encoding UV fluctuations in a redefinition of the classical action, without altering the physical content of the theory.

Chapter 2

Theoretical background

In this chapter we want to provide with an overview on the general theoretical framework that supports this work, and introduce the main concepts for the successive parts. Each section in this chapter is, by no means, meant as an exhaustive treatment. The description will be quite conceptual, rather than technical, and aims at recalling the main ideas and fix conventions. We ask the reader to consult appropriate references, which will be given in the corresponding sections, for a more detailed treatment of the topics.

2.1 The renormalisation group

Landau's mean field approach to study phase transition [8] gained wide popularity in the 1930's and 40's, since it was able to describe critical properties of many systems and it provided inspiration for the later Landau-Ginzburg theory of superconductivity [9]. Thus, it was soon proved to be inaccurate to predict some experimentally well proven properties of certain systems near their critical point [10]. This is because, beeing a mean field theory, it did not take into account the role of spatial fluctuations. The idea of block-spin transformation, systematically developed by Kadanoff [11], made a big step towards a deeper understanding of the scaling behaviour, and posed the basis for the later work of Wilson [12–14], which still constitutes the basis for modern approaches to renormalisation in field theory and statistical physics.

2.1.1 Block-spin RG

To illustrate the idea, let us consider a set of spins whose magnetisation is described by a function $\phi(x)$. The spins are located on a discrete lattice $\mathscr{L}$ with spacing a, so that the function assumes values only at such sites $\phi(x_i) = \phi_i \neq 0 \Leftrightarrow x_i \in \mathscr{L}$. Suppose then that their interaction is described by a certain action $S[\phi]$ and a partition function

$$Z = \sum_{\phi} \mathrm{e}^{-S[\phi]}.$$

We now want to introduce a coarse-grained (or blocked) field $\bar{\phi}$ within a spacetime cell of volume $\mathcal{V}$. Such a coarse grained field can be defined, for example, as an average over the spins within the cell $\mathcal{V}$. If the spins can only be 0 or 1 like in a Ising model, then we might opt for a majority rule [15]. We now want to find a new action S_b such that

$$Z = \sum_{\phi} \mathrm{e}^{-S(\phi)} = \sum_{\bar{\phi}} \mathrm{e}^{-S_b(\bar{\phi})}. \tag{2.1}$$

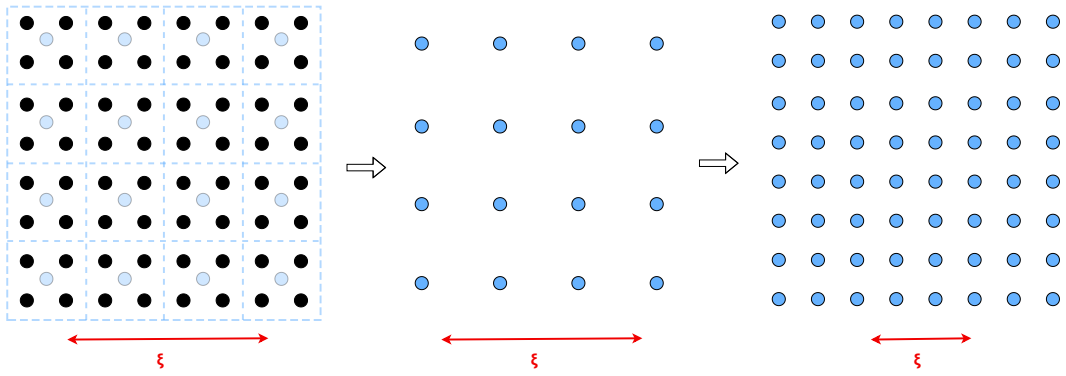

FIGURE 2.1: The two steps of the block-spin transformation. The black dots indicate the original field ϕ, while the blue dots indicate the coarse-grained field $\bar{\phi}$.

Suppose for the moment that such S_b has been found. The coarse-graining procedure comes with a loss of resolution since the spacing is changed $a \to 2a$. Hence one can rescale distances and momenta in the new action via $a \to a/2, p \to 2p$ and then compare the result with the initial action. This constitutes the second step of the block-spin transformation.
The whole procedure can be iterated multiple times, and can be thought as a zoom-out with a corresponding coarse graining, in order to describe the system in terms of the relevant scales as pictured in figure 2.1. As made clear in the picture, the physical correlation length ξ is reduced by the block-spin step, since the description is now in terms of the coarse field $\bar{\phi}$. There are only two exceptions for this, either the correlation length is zero, or infinite. The latter case represents a fixed-point of the RG, and the system exhibits scale invriance.
Note that the condition (2.1) is non-trivial. One can, in principle, build an ad-hoc action that fulfills the condition, but it is complicated, since S_b can be also be very different from S. For example, if the action $S[\phi]$ contains only nearest-neighbour interactions, the new action $S'[\bar{\phi}]$ can contain higher order interactions such as nearest-to-nearest neighbour, or even more. In principle, all the terms compatible with the original symmetries are allowed, and one has often to rely on some approximations. For example, if one is interested in long range properties of the system, and the volume $\mathcal{V}$ is sufficiently small, one can assume the functional form of the action S to remain approximately the same, with the the only change due to the dimensional rescaling of dimensionful quantities mentioned above. Thus, as the procedure is iterated and the correlation length scale is approached, one has to take account higher order interactions. For an example of the explicit construction of the RG for an Ising model, see [15].

2.1.2 Wilsonian RG

The Wilsonian picture of renormalisation [12, 13] is formulated in momentum space and in general is more suitable for theories in the continuum.
The idea is that a physical theory observed a energy scale Λ can be seen as an effective theory of a more fundamental one, defined at scale $\Lambda_0 > \Lambda$.
To see how this can happen, let us consider a theory defined by the action $S[\phi]$ scale Λ_0, and let us split the field as

$$\phi = \bar{\phi} + \varphi$$

where $\bar{\phi}$ are fields with momenta $p^2 \leq \Lambda^2$ and φ are fields with $\Lambda^2 < p^2 \leq \Lambda_0^2$.
This allows to split the action as

$$[\bar{\phi} + \varphi] = S_\Lambda[\bar{\phi}] + \delta S[\bar{\phi}, \varphi]$$

including all the dependence on φ in $\delta S[\bar{\phi}, \varphi]$.
The path integral can be rewritten as

$$\begin{aligned} Z = \int D\phi\, e^{-S[\phi]} &= \int D\bar{\phi}_\Lambda\, e^{-S_\Lambda[\phi]} \int D\varphi\, e^{-\delta S[\phi,\varphi]} \\ &= \int D\bar{\phi}_\Lambda\, e^{-S_\Lambda[\bar{\phi}] - S_{\mathrm{UV}}[\bar{\phi}]} \\ &= \int D\bar{\phi}_\Lambda\, e^{-S^{\mathrm{eff}}_\Lambda[\bar{\phi}]}, \end{aligned}$$

where

$$S^{\mathrm{eff}}_\Lambda = S_\Lambda[\bar{\phi}] + S_{\mathrm{UV}}[\bar{\phi}], \qquad S_{\mathrm{UV}}[\bar{\phi}] = -\log\left(\int D\varphi\, e^{-S_\Lambda[\phi,\varphi]}\right).$$

$S_{\mathrm{UV}}[\bar{\phi}]$ encodes all the information of UV modes with $\Lambda^2 < p^2 \leq \Lambda_0^2$.
The action $S_\Lambda[\bar{\phi}]$ has the same functional form of the initial action $S[\phi]$, but it is now defined only for fields with momenta $p^2 \leq \Lambda^2$. Instead, $S^{\mathrm{eff}}_\Lambda[\bar{\phi}]$ constitutes an effective description of the original theory at scale Λ and depends only on degrees of freedom with $p^2 \leq \Lambda^2$.
One can then operate a rescaling of distances and momenta to complete the Wilson RG step, according to the parameter

$$s^2 = \Lambda^2/\Lambda_0^2.$$

If, for example, d_g is the energy dimension of a coupling g in the action, then the rescaling transformation causes

$$g \to s^{d_g}\, g.$$

The same applies to the fields and other dimensionful quantities. If the corrections from S_{UV} are negligible, such as for high cutoff $\Lambda \approx \Lambda_0$, then this is the only contribution to the change in the couplings and fields due to the Wilson step. More in general, for higher order iterations of the procedure, the couplings' dependence on s is caputered by the β-functions

$$\beta_g = \frac{d}{ds}\, g(s).$$

A full treatment of RG is out of scope here and we ask the reader to consult more appropriate references fore more details [16].

At this point, one can clearly see the analogy with the block-spin transformation introduced in the previous section. Performing the integral over high momenta modes can be thought as performing averages (coarse graining) over neighbours. This causes a loss of resolution which can be recovered by rescaling distances and momenta. The rescaling is essential for a description of fixed points, since it can be pictured as a zoom-out.
Therefore, the philosophy of Kadanoff and Wilson approaches was that the blocking transformation reduces the complexity of many-body systems by systematically reducing the number of degrees of freedom being taken into account, without changing the physical content of the theory [7, 17].

We want to conclude this section by mentioning that the splitting of the action can be done by writing

$$S_\Lambda^{\text{eff}}[\bar{\phi}] = S[\phi] + \Delta S_\Lambda^{(\text{IR})}[\bar{\phi}],$$

where $\Delta S_\Lambda^{(\text{IR})}[\hat{\phi}]$ is a regulating function which typically assumes the form

$$\Delta S_\Lambda^{(\text{IR})}[\bar{\phi}] = \frac{1}{2}\int \frac{\mathrm{d}^d p}{(2\pi)^d}\bar{\phi}(-p)\,\Lambda^2\left(\frac{1}{r_\Lambda(p^2)} - 1\right)\bar{\phi}(p), \tag{2.2}$$

For a sharp momentum cutoff one has

$$r_\Lambda(p^2) = \theta\left(p^2 - \Lambda^2\right).$$

This result will allow for a deep connection between coloured stochastic quantisation and the functional renormalisation group, the latter describing the functional dependence of $S_\Lambda^{\text{eff}}[\bar{\phi}]$ on the cutoff scale Λ citationsssss.

2.2 Lattice QFT and the continuum limit

The starting set up is the euclidean formulation of quantum field theory, where one typically defines a path integral Z, which, for a general scalar field $\phi(x)$ and a fermion field $\psi(x)$, assumes the form

$$Z = \int \mathcal{D}\phi\mathcal{D}\psi\mathcal{D}\bar{\psi}\, e^{-S[\phi,\psi,\bar{\psi}]}, \qquad \mathcal{D}\xi = \prod_x d\xi_x, \quad \xi \in \{\phi,\psi,\bar{\psi}\}, \tag{2.3}$$

and correlation functions are computed via

$$\langle \xi_{x_1}\dots\xi_{x_n}\rangle = \frac{1}{Z}\int \mathcal{D}\phi\mathcal{D}\psi\mathcal{D}\bar{\psi}\,\xi_{x_1}\dots\xi_{x_n}\, e^{-S[\phi,\psi,\bar{\psi}]}, \qquad \xi_{x_i} \in \{\phi_{x_i},\psi_{x_i},\bar{\psi}_{x_i}\}.$$

Let us then consider a lattice $\mathscr{L}$, with spacing a, and N_μ points in each spacetime direction μ, hence a physical length $L_\mu = N_\mu\, a$. For simplicity we restricted here to a scalar field ϕ and we will recall fermionic properties only when relevant, but what follows has general validity. The action and the path integral measure are now taken over discrete quantities

$$\begin{aligned} S = \int d^d x\,\mathcal{L}(\phi(x)) \qquad &\to \qquad S = a^d \sum_{n\in\mathscr{L}} \mathcal{L}(\phi(n)), \\ \prod_x d\phi(x) \qquad &\to \qquad \prod_{n\in\mathscr{L}} d\phi(n), \end{aligned}$$

where $\mathcal{L}(\phi)$ is the Lagrangian density function.
The path integral is hence

$$Z = \int \prod_n d\phi(n)\, e^{-S[\phi]},$$

and the probability of a field configuration ϕ

$$p(\phi) = \frac{1}{Z}\, e^{-S[\phi]}. \tag{2.4}$$

Expectation value of observables are computes as

$$\langle O(\phi) \rangle = \frac{1}{Z} \int \prod_n d\phi(n)\, O(\phi)\, e^{-S[\phi]}. \tag{2.5}$$

In order to simulate a theory and perform the above sums one has to go to finite volumes and impose boundary conditions. In the space directions, we take periodic conditions

$$\phi(t, \vec{x}) = \phi(t, \vec{x} + \vec{T}),$$
$$\psi(t, \vec{x}) = \psi(t, \vec{x} + \vec{T}).$$

Instead, a finite time extent is related to the temperature of the system [2, 18] via

$$\beta = 1/T = 1/L_t,$$

and boundary conditions are chosen depending on the spin-statistic of the corresponding particles, namely periodic conditions for bosons, and anti-periodic for fermions

$$\begin{aligned} \phi(t, \vec{x}) &= \phi(t + T, \vec{x}) \qquad \text{bosons,} \\ \psi(t, \vec{x}) &= -\psi(t + T, \vec{x}) \quad \text{fermions.} \end{aligned}$$

Such a formulation naturally brings a momentum cutoff $\Lambda = \pi/a$ since now all the momenta are restricted to the first Brilloune zone $p_\mu \in [-\pi/a, \pi/a]$.

To compute observables one relies on Monte-Carlo methods to generate field configurations, sampling the distribution (2.4) and convergence to the statistical value given by (2.5) is expected in the limit of infinite samples $N_{\text{samp}} \to \infty$.
To recover the continuum results, one has to take $V \to \infty, a \to 0$ [1], but this task cannot be done so straightforwardly. Continuum limits of lattice theories are intimately connected to the existence of critical points. To see why this is the case, consider the dimensionless mass gap

$$\hat{\xi} = m\, a$$

of a certain theory. The quantity ξ is also called correlation length and it is related to the exponential decay of correlation functions between local observables measured at different points on the lattice, as given by add ref. eq.
When taking the continuum limit we want $a \to 0$, while having a finite physical mass m. This implies that the correlation length $\hat{\xi}$ has to diverge: in the language of statistical physics, this is a second order phase transition. Of course to bring the system at its critical point, where such phase transition happens, one has to tune the bare parameters g_0^i of the theory to their critical values $g_0^{i\,*}$. To do this, one should

[1] the order here is important, see for example [19, 20]

find the zeros of the lattice beta functions

$$\beta_g^{\text{latt}} = a\frac{d}{da}g(a) \stackrel{!}{=} 0, \qquad a = \pi/\Lambda.$$

As this is quite hard task to do on the lattice, one typically relies on some approximation schemes such as employing perturbative continuum beta functions.
In any case, from this description it should be clear that the spacing a should not be treated as a free parameter in the continuum limit, but rather a dynamically determined quantity that depends on the couplings of the theory.

Note that in the limit $a \to 0$, one has $\Lambda \to \infty$. If one's scope is to simulate an effective theory which is expected to hold only up to a scale Λ_{phys}, one must have $\Lambda \leq \Lambda_{\text{phys}}$, with a consequent lower bound on the lattice spacing $a \geq a_{\text{phys}} = \pi/\Lambda_{\text{phys}}$.

2.3 Stochastic quantisation

The idea of stochastic quantisation [21, 22] is that Euclidean Quantum Field theory can be thought as a system in thermal equilibrium with a heat reservoir and hence described as a stochastic process via the Langevin equation. For this, one has to introduce a fictitious time variable τ that labels the state $\phi(\tau, x)$ of the system during the evolution.

2.3.1 Standard stochastic quantisation

Let us consider, for example, a scalar field ϕ with a Euclidean action $S[\phi]$ and the following Langevin equation

$$\partial_\tau \phi(\tau, x) = -\frac{\delta S[\phi]}{\delta \phi(\tau, x)} + \eta(\tau, x), \tag{2.6}$$

where $K_\phi(\tau) \equiv -\delta S[\phi]/\delta\phi(\tau, x)$ is the drift term and $\eta(\tau, x)$ is a random white noise field assumed to be normally distributed

$$P(\eta) = \frac{\exp\left(-\frac{1}{4}\int_{\tau,x}\eta^2(\tau, x)\right)}{\int D\eta \exp\left(-\frac{1}{4}\int_{\tau,x}\eta^2(\tau, x)\right)},$$

which, in particular, implies

$$\langle \eta(x, \tau)\rangle = 0, \qquad \langle \eta(x, \tau)\,\eta(x', \tau')\rangle = 2\,\delta(x - x')\,\delta(\tau - \tau'). \tag{2.7}$$

Stochastic average with respect to the measure $P(\eta)$ are computed via

$$\langle A(\eta)\rangle = \int D\eta\, P(\eta)\, A(\eta).$$

In momentum space, (2.7) becomes

$$\begin{aligned}\langle \eta(p,\tau)\rangle &= \left\langle \int_x e^{ipx}\eta(x,\tau)\right\rangle = \int_x \left\langle e^{ipx}\eta(x,\tau)\right\rangle = 0,\\ \langle \eta(p,\tau)\eta(q,\tau')\rangle &= \left\langle \int_{xy} e^{ipx+iqy}\eta(x,\tau)\eta(y,\tau')\right\rangle\\ &= \int_{xy} e^{ipx+iqy}\left\langle \eta(x,\tau)\eta(y,\tau')\right\rangle\\ &= 2\,(2\pi)^2\,\delta(p+q)\,\delta(\tau-\tau').\end{aligned} \tag{2.8}$$

In absence of the noise term $\eta(\tau,x)$, equation (2.6) simply represents an evolution of the field towards the minimum of the action, and at equilibrium the field is constrained to $\partial_\tau\phi(x,\tau) = 0 = \delta S[\phi]/\delta\phi(\tau,x)$, namely to the classical equations of motion.
For any observable O, which is function of the field, one has, for fixed time τ,

$$\langle O(\phi(\tau))\rangle = \int D\eta\, P(\eta)\, O(\phi(\tau)),$$

from which it follows straightforwardly using the Langevin equation and $\langle\eta\rangle = 0$

$$\frac{d}{d\tau}\langle O(\phi(\tau))\rangle = \left\langle \frac{\delta O}{\delta\phi(\tau,x)}\,\partial_\tau\phi(\tau,x)\right\rangle = -\left\langle \frac{\delta O}{\delta\phi}(\tau,x)\,\frac{\delta S}{\delta\phi(\tau,x)}\right\rangle.$$

It follows trivially that for $O(\phi(\tau)) = \phi(\tau,x)$

$$\frac{d}{d\tau}\langle\phi(\tau,x)\rangle = -\left\langle\frac{\delta S}{\delta\phi(\tau,x)}\right\rangle \quad \underset{Equilibrium}{\Longrightarrow} \quad \left\langle\frac{\delta S}{\delta\phi(\tau,x)}\right\rangle = 0.$$

This also provides a consistency check for the correct implementation of the simulation, since the drift $K_\phi = -\delta S/\delta\phi$ is computed numerically during the evolution.
More generally, one can derive a correspondent Fokker-Planck equation [23], which can be proven to have a stationary distribution if the action is bounded from below, given by [22]

$$\mathcal{P}(\phi) = \frac{1}{Z}\,\exp\left(-S[\phi]\right). \tag{2.9}$$

This allows one to compute correlation functions as moments of the probability distribution (2.9). In particular, one has

$$\langle O\rangle_{P(\eta)} = \langle O\rangle_{\mathcal{P}(\phi)} \equiv \langle O\rangle. \tag{2.10}$$

2.3.2 Stochastic quantisation with coloured noise

In the stochastic quantisation procedure the noise which accounts for the quantum fluctuations of the theory is assumed to be white, as defined in equations (2.7), (2.8). We now want to examine the dynamics in presence of a coloured noise, writing the Langevin equation as

$$\partial_\tau\phi(x,\tau) = -\frac{\delta S[\phi]}{\delta\phi(\tau,x)} + \eta_{\rm col}(x,\tau),$$

with $\eta_{\rm col}(x,\tau) = r_\Lambda(x)\,\eta(x,\tau)$. In particular, here we restrict to the regulating function defined as a sharp cutoff in momentum space

$$r_\Lambda(p) = \theta(\Lambda^2 - p^2), \tag{2.11}$$

and we invite the reader to consult [24] for a discussion of other regulating functions. The noise field in momentum space is then

$$\begin{aligned}\eta_{\rm col}(p,\tau) &= \mathcal{F}[\eta_{\rm col}(x,\tau)] = \mathcal{F}[r_\Lambda(x,\tau)\eta(x,\tau)] = \mathcal{F}[r_\Lambda(x,\tau)] \star \mathcal{F}[\eta(x,\tau)] \\ &= \theta(\Lambda^2 - p^2)\,\eta(p,\tau).\end{aligned}$$

where $\mathcal{F}$ indicates the Fourier transform and $\star$ the convolution product.
An interesting quantity to look at is the position-space noise correlation function

$$\begin{aligned}C_\eta(x,\tau,y,\tau') &= \langle \eta_{\rm col}(x,\tau)\,\eta_{\rm col}(y,\tau')\rangle \\ &= \frac{1}{(2\pi)^4}\int D\eta\, P(\eta)\left[\int_{p,q} e^{-ipx-iqy}\eta_{\rm col}(p,\tau)\,\eta_{\rm col}(q,\tau')\right] \\ &= \frac{1}{(2\pi)^4}\int_{p,q} e^{-ipx-iqy}\int D\eta\,\left[P(\eta)\,\eta(p,\tau)\,\eta(q,\tau')\right] \\ &\quad \times \theta(\Lambda^2-p^2)\,\theta(\Lambda^2-q^2) \\ &= \frac{2}{(2\pi)^2}\int_{p,q} e^{-ipx-iqy}\,\delta(p+q)\,\theta(\Lambda^2-p^2)\,\theta(\Lambda^2-q^2)\,\delta(\tau-\tau') \\ &= \frac{2}{(2\pi)^2}\int_p e^{-ip(x-y)}\,\theta(\Lambda^2-p^2) = \frac{1}{\pi}\int_0^\Lambda d\omega\,\omega\,J_0(\omega|x-y|),\end{aligned} \tag{2.12}$$

where $J_0(x)$ is a Bessel function of the first order. The integral in the last line is computed numerically as a function of $d = |x-y|$ and reported in figure 2.2 for three different values of the cutoff $\Lambda_1 < \Lambda_2 < \Lambda_3$. This shows nicely that for $|x-y| \ll 1/\Lambda$ the noise is now correlated, while for $|x-y| \gg 1/\Lambda$ the correlation function vanishes, as in the white noise case. In other words, only the short-length behaviour of the system is affected by the introduction of such a regulating term, as one could expect.

Another intuitive and interesting aspect of the dynamics in the presence of coloured noise can be deduce by looking at the field expression in terms of the retarded Langevin Green function [22], which is here not derived, but reported from [24]

$$\phi(x,\tau) = \int_{x'}\int_{-\infty}^{\tau} \mathrm{d}\tau' G\left(x-x',\tau-\tau'\right)\left[r_\Lambda\left(\Delta_x\right)\eta\left(x,\tau'\right) - \frac{\delta S}{\delta\phi}|_{p=0}\,\phi\left(x',\tau\right)\right],$$

where

$$G\left(x-x',\tau-\tau'\right) = \theta\left(\tau-\tau'\right)\int_p \mathrm{e}^{-ip\cdot(x-x')}\mathrm{e}^{-(\tau-\tau')\left(p^2+m^2\right)}.$$

By looking at the first term in the square bracket, one can conclude that there is no propagation of modes with momentum $p^2 \geq \Lambda^2$ due to the noise term, but one can still have contribution from modes $p^2 > \Lambda^2$ from the second term, which corresponds to the deterministic part of the equations of motion. Stated differently, UV quantum fluctuations with $p^2 > \Lambda^2$ are removed from the dynamics of ϕ, but still contribute classically.

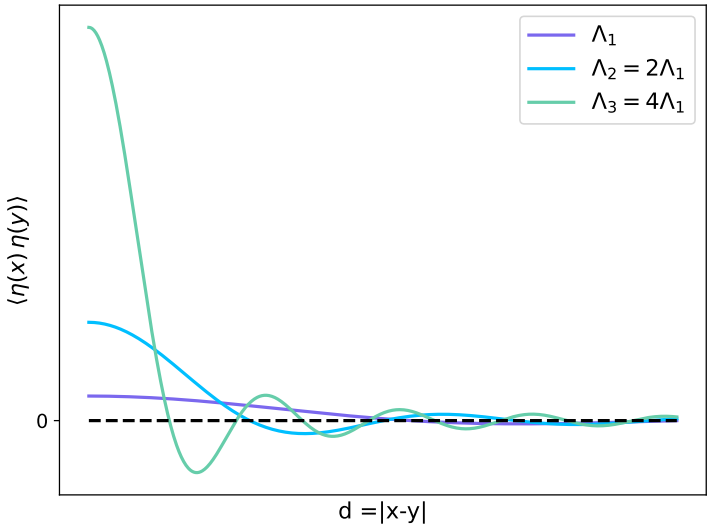

FIGURE 2.2: Noise correlation as a function of $d = |x - y|$ for three different values of the cutoff $\Lambda_1 < \Lambda_2 < \Lambda_3$, in arbitrary units. The plot is qualitative, but shows clearly that with a regulated noise, only the short-distance behaviour is affected.

Generally speaking, the stationary distribution probability of the regulated stochastic process is given by [24]

$$\mathcal{P}_\Lambda(\phi) = \frac{1}{Z} \exp\left(-S_\Lambda[\phi]\right) = \frac{1}{Z} \exp\left(-(S[\phi] + \Delta S_\Lambda[\phi])\right), \tag{2.13}$$

where the correction term $\Delta S_\Lambda[\phi]$, reads, for a regulator $r_\Lambda(p^2)$,

$$\Delta S_\Lambda[\phi] = \frac{1}{2} \int_p \phi_p \, \Lambda^2 \left(\frac{1}{r_\Lambda\left(p^2\right)} - 1 \right) \phi_{-p}.$$

at this point mention that this is the stationary pdf that one gets with frg for sharp cutoff, and cite some papers.

2.4 Chiral symmetry

In this section we want to introduce chiral symmetry and its breaking, both in the continuum and on the lattice.
It is useful to adopt the notation

$$\psi = (\psi^{(1)}, \ldots, \psi^{(N_f)}).$$

We then introduce left-handed and right-handed spinors

$$\psi_L = (1 - \gamma_5)\, \psi, \qquad \psi_R = (1 + \gamma_5)\, \psi,$$

for which

$$\psi = \frac{(1 - \gamma_5)}{2} \psi + \frac{(1 + \gamma_5)}{2} \psi = \psi_L + \psi_R.$$

2.4.1 Chiral symmetry in the continuum

The free massless Dirac Lagrangian

$$\mathcal{L}_D = \bar{\psi}\partial\!\!\!/\psi = \bar{\psi}_L\partial\!\!\!/\psi_L + \bar{\psi}_R\partial\!\!\!/\psi_R \tag{2.14}$$

is symmetric under the chiral group $SU(N_f)_L \times SU(N_f)_R$, namely

$$\begin{aligned} \psi_L(x) &\to U_L\psi_L(x), \qquad \bar{\psi}_L(x) \to \bar{\psi}_L(x)U_L^\dagger, \\ \psi_R(x) &\to U_R\psi_R(x), \qquad \bar{\psi}_R(x) \to \bar{\psi}_R(x)U_R^\dagger, \end{aligned}$$

for $U_L, U_R \in SU(N_f)$.
In terms of the full spinor ψ, the chiral symmetry can be written as

$$\psi \to M\psi, \qquad \bar{\psi} \to \bar{\psi},$$

where

$$M = e^{i(\theta_a\tau^a + \gamma_5\beta_a\tau^a)}, \quad \tau^a \in su(N_f)$$

so that

$$SU(N_f)_L \times SU(N_f)_R \simeq SU(N_f)_V \times SU(N_f)_A.$$

$SU(N_f)_V$ is the isospin subgroup, characterised by $\beta_a = 0$, and $SU(N_f)_A$ is the axial rotation subgroup, characterised by $\theta_a = 0$.
To be more precise, the full invariance group of the classical action is

$$SU(N_f)_L \times SU(N_f)_R \times U(1)_A \times U(1)_V,$$

where the axial and vector symmetry transformations are, respectively,

$$\psi \to e^{i\theta\gamma_5}\psi, \qquad \psi \to e^{i\theta}\psi.$$

One can thus prove that axial symmetry is broken by quantum anomalies (see for example [25]), so that the symmetry in the quantum case is

$$SU(N_f)_L \times SU(N_f)_R \times U(1)_V.$$

If equal masses for each flavour are introduced, then the symmetry group reduces to the isospin subgroup, diagonal in flavour space

$$SU(N_f)_V \times U(1)_V.$$

Finally, if the fermions have different masses, the symmetry group reduces to

$$\underbrace{U(1) \times \cdots \times U(1)}_{N_f} \times U(1)_V.$$

2.4.2 Chiral symmetry on the lattice

The essence of chiral symmetry for fermions can be expressed as [3]

$$\{\gamma_5, D\} = 0 \tag{2.15}$$

Implementing chiral symmetry on a finite-volume spacetime lattice, is a hard task. This is because, as proven by Nielsen and Ninomiya [26], one either has chiral symmetry on the lattice, or solves the doubling problem.
In particular, the insertion of the Wilson term in the action, as shown in Appendix B, causes explicit breaking of the chiral symmetry. If one's goal is to study spontaneous symmetry breaking, this constitues a problem. Thus, many options have been proposed to circumvent the issue. As an example we mention the approach by Ginsparg and Wilson citationsssss, who proposed to modify the chiral symmetry condition (2.4) to

$$\{\gamma_5, D\} = a\, D\gamma_5 D$$

The right hand-side of the equation vanishes in the continuum limit $a \to 0$. In this way, one can define chiral symmetry on the lattice remaining consistent in the continuum limit. This approach will not be pursued further and we ask the reader to consult appropriate references [2, 3] for a detailed treatment.
Our approach to study chiral symmetry will be discussed and motivated in section 5.2.

2.5 Yukawa theory

2.5.1 Description of the model

Let us consider the Yukawa theory defined by the action

$$\begin{aligned} S[\phi,\psi,\bar\psi] &= S_\phi[\phi] + S_\psi[\psi,\bar\psi] + S_{\text{int}}[\phi,\psi,\bar\psi], \\ S_\phi[\phi] &= \int_x \phi_x \left(-\frac{\partial_x^2}{2} + \frac{m_\phi^2}{2}\right)\phi_x + \frac{\lambda}{4!}\,\phi_x^4, \\ S_\psi[\psi,\bar\psi] &= \int_x \sum_{f=1}^{N_f} \bar\psi_x^{(f)}\left(\not\partial_x + m_q\right)\psi_x^{(f)}, \\ S_{\text{int}}[\phi,\psi,\bar\psi] &= \int_x \sum_{f=1}^{N_f} g\,\bar\psi_x^{(f)}\,\phi_x\,\psi_x^{(f)}. \end{aligned} \tag{2.16}$$

One can see that the action is made of a scalar part $S_\phi[\phi]$, a fermionic part $S_\psi[\psi,\bar\psi]$ and a Yukawa interaction term $S_{\text{int}}[\phi,\psi,\bar\psi]$.
In pratice we will work with fixed number of flavours $N_f = 2$, but it is useful to keep track of N_f and set it to its value when needed.
It is also convenient for later purposes to define the operators K, D represented in position space as

$$\begin{aligned} K(x,y) &= \left(-\partial_x^2 + m_\phi^2\right)\,\delta(x,y), \\ D(x,y) &= \left(\not\partial_x + m_q + g\phi\right)\,\delta(x,y), \end{aligned} \tag{2.17}$$

and in momentum space as

$$\begin{aligned} \widetilde K(p,q) &= \int_{x,y} e^{-ipx}\left(\partial_x^2 + m_\phi^2\right)\,\delta(x,y)\,e^{iqy} = \left(\frac{p^2}{2} + \frac{m_\phi^2}{2}\right)\,\delta(p,q), \\ \widetilde D(p,q) &= \int_{x,y} e^{-ipx}\left(\not\partial_x + m_q + g\phi\right)\,\delta(x,y)\,e^{iqy} = \left(\not p_x + m_q + g\phi\right)\,\delta(p,q). \end{aligned} \tag{2.18}$$

This allows one to rewrite the action as

$$S[\phi,\psi,\bar{\psi}] = \int_x \frac{1}{2}\,\phi_x\,K_{xx}\,\phi_x + \frac{\lambda}{4!}\,\phi_x^4 + \sum_{f=1}^{N_f}\bar{\psi}_x^{(f)}\,D_{xx}\,\psi_x^{(f)}.$$

2.5.2 Chiral symmetry in the Yukawa model

The action written in terms of ψ_L, ψ_R, reads

$$S = S_\phi + \int_x \left[\bar{\psi}_L\,D\,\psi_L + \bar{\psi}_R\,D\,\psi_R + (m_q + g\phi)\;(\bar{\psi}_L\psi_R + \bar{\psi}_R\psi_L)\right]. \tag{2.19}$$

The action is not invariant under the full chiral group, but if $m_q = 0$ it is symmetric under the discrete chiral transformation

$$\begin{aligned} \phi &\to -\phi, \\ \psi_L \to \gamma_5\psi_L, &\qquad \bar{\psi}_L \to -\bar{\psi}_L\gamma_5, \\ \psi_R \to \gamma_5\psi_R, &\qquad \bar{\psi}_R \to -\bar{\psi}_R\gamma_5, \end{aligned}$$

which was first introduced in the Gross-Neveu model citationsssss. In order to generalise the model to the full chiral group, one has to consider an $O(4)$ scalar sector and interactions, since $O(4) \simeq SU(2) \times SU(2)$. Similar effective theories with such properties are, for example, the Nambu-Jona-Lasinio model and the Quark-Meson model citationssssss. Thus, since we are in $1+1$ dimensions, spontaneous breaking of continuous symmetries is forbidden by the Mermin-Wagner theorem citationsssss, and we decided to opt for a simple Yukawa theory.

We now want to discuss more in detail the phenomenom of (discrete) chiral symmetry breaking and how it can happen in the model. In fact, the latter can happen either explicitly in the classical action, if a finite quark mass is added, or spontaneously, if $\langle\phi\rangle \neq 0$.
To better see this, let us perform the fermionic path integral explicitly

$$\int \mathcal{D}\bar{\psi}\mathcal{D}\psi\;\exp\left(-\int_x \sum_{f=1}^{N_f}\bar{\psi}_x^{(f)}\,D\,\psi_x^{(f)}\right) = (\det D[\phi])^{N_f} = e^{N_f\,\mathrm{Tr}\,\log(D[\phi])},$$

where the trace is performed over spacetime and spinor components.
The full path integral can now be expressed in terms of the resulting effective action for the scalar fields

$$Z = \int \mathcal{D}\phi\; e^{-S_{\mathrm{eff}}[\phi]},$$

with

$$S_{\mathrm{eff}}[\phi] = S_\phi[\phi] - N_f \operatorname*{Tr}_{x,s} \log D[\phi]. \tag{2.20}$$

One can derive the classical equations of motion by imposing $\frac{\delta S}{\delta\phi} = 0$, here expressed in momentum space

$$(k^2 + m_\phi^2)\,\phi(x) + \frac{\lambda}{6}\,\phi^3(x) = N_f\,g\operatorname*{Tr}_s\left[D^{-1}(\phi(x))\right] = -N_f\,g\,\bar{\psi}(x)\psi(x) \tag{2.21}$$

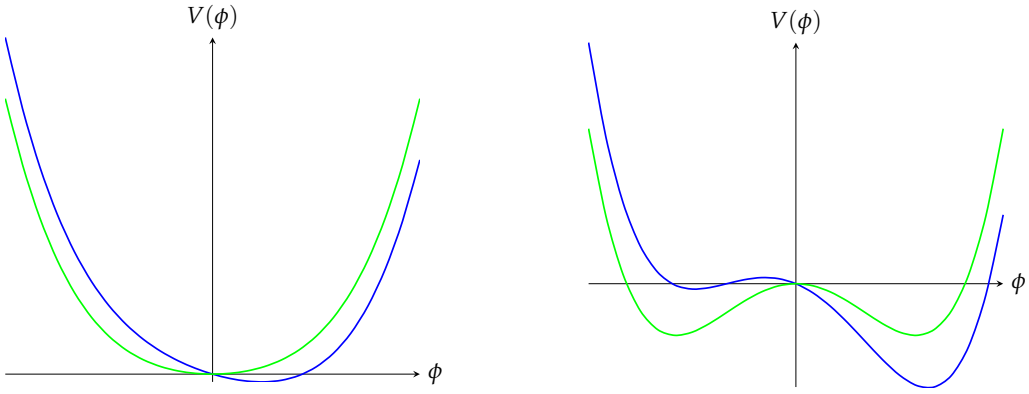

FIGURE 2.3: The introduction of the boson-fermion interaction, with a finite fermionic mass, causes explicit breaking of chiral symmetry, with consequence spontaneous breaking of the O(1) symmetry according to (2.23). It shifts the equilibrium position in the symmetric phase (left) causing $\langle\phi\rangle \neq 0$, and tilts the potential in the broken phase (right), making the two minima not equivalent.

For $\lambda = 0$, they highlight a simple proportionality relation between magnetisation and chiral condensate, which reads

$$\phi = -\frac{N_f\, g}{k^2 + m_\phi^2}\ \bar{\psi}\psi. \tag{2.22}$$

This relation, which was here derived at the classical level, is proven to hold also in mean field on the quantum level [27] and makes apparent the role of ϕ as a quark bilinear.
When bosons self-interactions are added, namely when $\lambda \neq 0$, the full relation between ϕ and the chiral condensate $\bar{\psi}\psi$ is given by (2.22), but still one expects, qualitatively,

$$\langle\phi\rangle \sim \langle\bar{\psi}\psi\rangle\,. \tag{2.23}$$

A non-vanishing condensate is also related to a physical quark mass [27, 28], while the presence of magnetisation causes the breaking of $O(1)$ symmetry. If $\langle\phi\rangle = v$, one can write $\phi(x) = v + \varphi(x)$ and the massless lagrangian assumes the form

$$S = S_\phi + \int_x [\bar{\psi}_L\, D\, \psi_L + \bar{\psi}_R\, D\, \psi_R + g v\ (\bar{\psi}_L\psi_R + \bar{\psi}_R\psi_L)] + g\varphi(x)\ (\bar{\psi}_L\psi_R + \bar{\psi}_R\psi_L) \tag{2.24}$$

hence showing that one can expect

$$\langle\phi\rangle \sim \langle\bar{\psi}\psi\rangle \sim m_q. \tag{2.25}$$

2.5.3 Phase structure and order parameters

We want to conclude this chapter by commenting on the phase strcture of the Yukawa theory. This will guide the choice of parameters for the investigation carried in the remaining sections. A sketch of the different phases of the model is reported in figure 2.4. The order parameters are the magnetisation $M = \langle\phi\rangle$ and the staggered

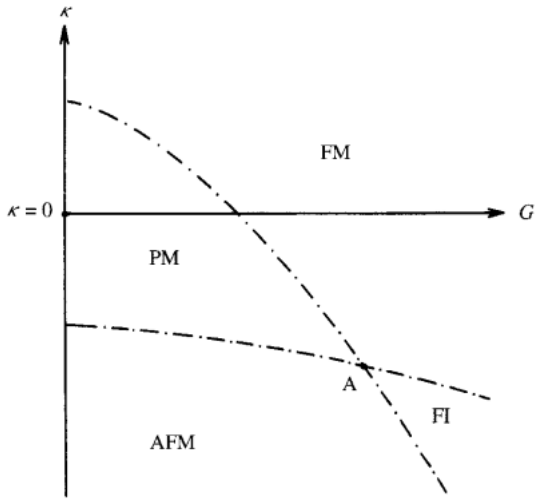

FIGURE 2.4: General phase diagram of a Yukawa theory.
I know that I wouldn't be allowed to use this picture, I will see later what to do.

magnetisation $M_s = \langle \Phi \rangle$, where

$$\Phi_x \equiv (-1)^{t+x} \phi_x = \mathrm{e}^{\mathrm{i}\pi(t+x)} \phi_x. \tag{2.26}$$

The four different phases are characterised by the following combinations of the order parameters

- paramagnetic phase: $M = 0, M_s = 0$,
- ferromagnetic phase: $M \neq 0, M_s = 0$,
- anti-ferromagnetic phase: $M = 0, M_s \neq 0$,
- ferrimagnetic phase: $M \neq 0, M_s \neq 0$.

The lattice observables used for the investigation are introduced in section 3.4.

Chapter 3

Methods and algorithms

3.1 Discretisation of the Yukawa theory

In order to make the theory suitable for a numerical simulation on a computer, the continuum formulation of the Yukawa model, which has been introduced in section 2.5, has to be discretised. Here we provided a sketch of a discretisation procedure, and we refer to other resources [1–4] for further details.

For what concerns the bosonic part of the action, a discretisation can be done straightforwardly with the following replacements

$$\begin{aligned} \int d^x \quad &\to \quad a^2 \sum_x, \\ \partial_t^2 + \partial_x^2 = \frac{\partial^2}{\partial t^2} + \frac{\partial^2}{\partial x_1^2} \quad &\to \quad \sum_\mu \left[\frac{\delta_{m,n+\mu} + \delta_{m,n-\mu} - 2\delta_{m,n}}{a^2} \right], \end{aligned}$$

which yields to the lattice action

$$\begin{aligned} S_\phi[\phi] &= a^2 \left(\frac{1}{2} \sum_{m,n} \phi_m \, K_{mn} \, \phi_n + \frac{\lambda}{4!} \sum_n \phi_n^4 \right) \\ &= \frac{1}{2} \sum_{m,n} \hat{\phi}_m \, \widehat{K}_{mn} \, \hat{\phi}_n + \frac{\hat{\lambda}}{4!} \sum_n \hat{\phi}_n^4, \end{aligned}$$

where we expressed everything in dimensionless quantities

$$\begin{aligned} \hat{m}_\phi^2 &= a^2 \, m_\phi^2, \\ \hat{\lambda} &= a^2 \, \lambda, \\ \widehat{K}_{mn} &= a^2 K_{mn}. \end{aligned} \tag{3.1}$$

The operator components $\widehat{K}_{mn}$ are the discretised version of (2.17)

$$\widehat{K}_{mn} = -\sum_\mu \left[\delta_{m,n+\mu} + \delta_{m,n-\mu} - 2\,\delta_{m,n} \right] + \hat{m}_\phi^2 \, \delta_{mn} \tag{3.2}$$

and its representation in momentum space is

$$\begin{aligned}\widehat{K}_{p,q} &= \sum_{n,m} e^{ipn}\,\widehat{K}_{nm}\,e^{-iqm} \\ &= \sum_{n,m} e^{ipn}\left(-\sum_{\mu}\left[\delta_{m,m+\mu}+\delta_{m,m-\mu}-2\delta_{m,n}\right]+\hat{m}_{\phi}^{2}\,\delta_{mn}\right)e^{-iqm} \\ &= \sum_{n} e^{i(p-q)n}\left[\hat{m}_{\phi}^{2}+2\sum_{\mu}\left(1-\cos\left(q_{\mu}\right)\right)\right] \\ &= \left[\hat{m}_{\phi}^{2}+\sum_{\mu}4\sin^{2}\left(\frac{p_{\mu}}{2}\right)\right]\,\delta(p-q).\end{aligned}$$

For what concerns the fermionic action, a naïve discretisation is not sufficient, due to the well known doubling problem [1, 2]. In this work Wilson fermions [29] are employed as a way to fix such issue. Details of this formulation are explained in Appendix B. Here, only the final discretised action is reported, which reads

$$S_{\psi}\left[\hat{\psi},\hat{\bar{\psi}}\right]+S_{\text{int}}\left[\hat{\phi},\hat{\psi},\hat{\bar{\psi}}\right]=\sum_{f=1}^{N_f}\hat{\bar{\psi}}_{m}^{(f)}\,\widehat{D}_{mn}\,\hat{\psi}_{n}^{(f)}, \tag{3.3}$$

with ψ_n beeing a two-component spinor, and $\widehat{D}_{m,n}$ the Wilson-Dirac operator defined as

$$\begin{aligned}\widehat{D}_{m,n} = &-\left(\frac{\Gamma_{+\hat{0}}}{2}\,\delta_{m,m+\hat{0}}+\frac{\Gamma_{-\hat{0}}}{2}\,\delta_{m,m-\hat{0}}+\frac{\Gamma_{+\hat{1}}}{2}\,\delta_{m,m+\hat{1}}+\frac{\Gamma_{-\hat{1}}}{2}\,\delta_{m,m-\hat{1}}\right) \\ &+\left(2ar+\hat{m}+\hat{g}\phi\right)\,\delta_{s,s'}\,\delta_{m,n}.\end{aligned} \tag{3.4}$$

Note that the interaction term $g\,\bar{\psi}\phi\psi$ has been included in the definition of D.
The Wilson projectors $\Gamma_{\pm\hat{\mu}}$ are defined as

$$\Gamma_{\pm\hat{\mu}} = ar\,\mathbb{1}_s \mp \gamma_{\mu}.$$

Since $r \in [0,1]$ is a free parameter, in this work we set $r = 1$, if not otherwise specified.
In summary the discretised action for the Yukawa model is

$$S\left[\hat{\phi},\hat{\psi},\hat{\bar{\psi}}\right]=\sum_{m,n}\hat{\phi}_{m}\,\widehat{K}_{m,n}\,\hat{\phi}_{n}+\frac{\hat{\lambda}}{4!}\,\hat{\phi}_{m}^{4}\,\delta_{m,n}+\sum_{f=1}^{N_f}\hat{\bar{\psi}}_{m}^{(f)}\,\widehat{D}_{mn}\hat{\psi}_{n}^{(f)}, \tag{3.5}$$

with $\widehat{K}_{mn}, \widehat{D}_{mn}$ given respectively by (3.2) and (3.4).
For later reference, we also report the discretised version of the effective action (2.20)

$$\begin{aligned}S_{\text{eff}}[\hat{\phi}] &= S_{\phi}[\hat{\phi}]-N_f\operatorname*{Tr}_{n,s}\log\widehat{D} \\ &= \sum_{m,n}\hat{\phi}_{m}\,\widehat{K}_{m,n}\,\hat{\phi}_{n}+\frac{\hat{\lambda}}{4!}\,\hat{\phi}_{m}^{4}\,\delta_{m,n}-N_f\operatorname*{Tr}_{n,s}\log\widehat{D}_{nn}.\end{aligned} \tag{3.6}$$

The full discrete path-integral reads

$$Z=\int\prod_{n}d\hat{\phi}_{n}\,e^{-S_{\text{eff}}[\hat{\phi}]}. \tag{3.7}$$

In the remaining of this work, both the original action S and the effective action S_{eff} will be denoted by S for simplicity. It will be clear from the context which of the two we will be referring to.

3.2 Langevin Monte Carlo

The relations (**??**) suggest that equation (2.6) can be integrated numerically for discrete time steps τ_n to generate field configurations distributed according to (2.9). The simplest first-order integration algorithm is the Euler-Majorana scheme [21]

$$\phi(\tau_{n+1}, x) = \phi(\tau_n, x) - \epsilon \frac{\delta S[\phi]}{\delta \phi(\tau_n, x)} + \sqrt{\epsilon}\, \eta(\tau_n, x) + O(\epsilon^2),$$

where $\epsilon = \tau_{n+1} - \tau_n$. Higher order integration schemes are possible (see e.g.[30, 31]), but not adopted in this work, and an adaptive step size is employed as detailed in Appendix C. In this way, for any observable O, one can introduce a Monte-Carlo estimator $\langle O \rangle_*$ which converges to the expectiation value given by (2.10) in the limit of infinite samples

$$\langle O \rangle_* = \frac{1}{N_{\text{samp}}} \sum_{i=1}^{N_{\text{samp}}} O_i \quad \underset{N_{\text{samp}} \to \infty}{\longrightarrow} \quad \langle O \rangle = \frac{1}{Z} \int D\phi\, O(\phi)\, \exp\left(-S[\phi]\right), \tag{3.8}$$

where $O_i = O(\phi(\tau_i))$ is the sample of the observable O done at time τ_i.

For the discretised action of the Yukawa theory (3.6) the drift reads, explicitly,

$$\begin{aligned} \frac{\partial S}{\partial \hat{\phi}_m(\tau_n)} &= \frac{\partial S_{\hat{\phi}}}{\partial \hat{\phi}_m(\tau_n)} - N_f \operatorname*{Tr}_s \left[\sum_{j,k} \widehat{D}^{-1}_{jk} \frac{\partial \widehat{D}_{kj}(\hat{\phi})}{\partial \hat{\phi}_m(\tau_n)} \right] \\ &= \sum_l \widehat{K}_{ml}\, \hat{\phi}_l + \frac{\hat{\lambda}}{6} \hat{\phi}_m^3 - \hat{g}\, N_f \operatorname*{Tr}_s \left[(\widehat{D}_{mm})^{-1}(\hat{\phi}(\tau_n)) \right]. \end{aligned} \tag{3.9}$$

While the bosonic contribution can be computed in a straightforward manner, the computation of the fermionc contribution requires the inversion of the Dirac operator. This, in general, cannot be done straightforwardly, mainly due to computational reasons. In fact, the full Dirac operator would be a $(2 \cdot N_t \cdot N_x \cdot N_f)^2$ dimensional object and a full inversion would be very expensive. In fact, D^{-1} has to be recomputed at every step and the best available algorithm as today for the matrix inversion has a computational complexity of $O(n^{2.371552})$ [32]. To circumvent this, we use the bilinear noise scheme [30, 33] which is illustrated in Appendix C.

3.3 Applications of coloured noise in lattice QFT

After the general introduction on coloured noise given in the previous paragraph, let us now look more closely on the lattice formulation and at some possible applications of the technique, some of which will be studied numerically in chapter **??**.

To this end, let us consider a two-dimensional lattice with side lengths L_t, L_x and spacing $a = a_x = a_t$. This implies a maximum momentum $p_{\max} = \pi/a$ in each spacetime direction and $N_x = L_x/a, N_t = L_t/a$ points in each direction. Let us also define

$$\Lambda_0^2 \equiv (p^x_{\max})^2 + (p^t_{\max})^2, \tag{3.10}$$

which indicates the maximum squared momentum on the given lattice.
We then consider a simulation with a regularised noise defined by a cutoff $\Lambda \leq \Lambda_0$ and we define a dimensionless parameter

$$s^2 = \frac{\Lambda^2}{\Lambda_0^2}, \qquad 0 \leq s \leq 1. \tag{3.11}$$

Note that Λ implicitly defines a length scale given by $a_{\text{eff}} = \pi/\Lambda$.

3.3.1 Classical-to-quantum interpolation

The use of coloured noise, allows for a smooth interpolation between the fully classical and fully quantum picture. In fact, one can perform various simulations changing the value of the cutoff fraction s and adding or removing quantum degrees of freedom, as pictured in figure add figure. This can be used either to investigate the role of quantum fluctuations in the system, or to remove irrelevant degrees of freedom, resulting in a speed-up of the simulation.

3.3.2 Noise-induced transition

Noise-induced transition is a well known field of stochastic dynamics [23, 34, 35] and consists in investigating whether noise can qualitatively affect the behaviour of a system. In our case, since noise is due to quantum fluctuations, we are interested in understanding if quantum fluctuations can trigger a phase transition with respect to the classical system, with the same parameters settings.
This question will be addressed in section 5.2 and it will be shown that for small negative bosonic mass, the classical system lies in a state of broken symmetry, while in the quantum case, the symmetry is restored.

3.3.3 Cooling and the continuum limit of effective theories

Following the paradigm of Kadanoff-Wilson of chapter 2, we want to use RG properties to encode quantum fluctuations in a redefinition of the couplings of the bare action. This removes short-distance fluctuations from the simulation, without changing the physical content of the theory. Note that this would, in principle, require a detailed knowledge of the β-functions of the theory. Thus, for sufficiently high cutoff, approximate Ansatz such as dimensional rescalings are generally enough. We will pursue this way, as follows.

Let us consider a simulation with $s = 1$ and a set of bare couplings $\{g_0^i\}$, and another simulation with $s' < 1$ and new set of couplings $\{g_0^{i\prime}\}$.
For what concerns the scalar part of the action, a dimensional rescaling, which corresponds to a tree-level RG transformation, is rather straightforward

$$\hat{m}_\phi^2 = (a^2 m_\phi^2) \;\to\; s^2(a^2 m_\phi^2) = s^2\,\hat{m}_\phi^2, \qquad \hat{\lambda} = (a^2\lambda) \;\to\; s^2(a^2\lambda) = s^2\hat{\lambda},$$
$$\hat{\phi} = \phi \;\to\; \phi = \hat{\phi}.$$

The fermionic part needs some more careful analysis. For simplicity, let us for the moment set $N_f = 1$.
In a lattice simulation one wants to perform the integral over the fermionic fields and works with the effective action (2.20). In this case the drift is given by equation (3.9), with the fermionic contribution

$$K_\psi = g \operatorname*{Tr}_s D^{-1}, \tag{3.12}$$

or, in terms of dimensionless quantities,

$$\widehat{K}_\psi = (ag) \operatorname*{Tr}_s (aD)^{-1}.$$

This implies that under a lattice block-spin transformation, where $a \to sa$,

$$\widehat{K}_\psi \to (sag) \operatorname*{Tr}_s (saD)^{-1} = \widehat{K}_\psi. \tag{3.13}$$

On the other side, when computing the drift via the original action (2.16), one gets

$$\begin{aligned} K = -\frac{\delta S}{\delta\phi} &= K_\phi - g\,\bar{\psi}\psi = \\ &= -\hat{K}_{mn}\,\phi_n - \frac{\lambda}{6}\,\phi^3 - g\,\bar{\psi}\psi. \end{aligned} \tag{3.14}$$

where, in the last row, $\widehat{K}_{mn}$ indicates the bosonic operator components (3.2).
The fermionic contribution is given by

$$K'_\psi = -g\,\bar{\psi}\psi.$$

Note that all the terms in the equation (3.14) have dimension 2, in units of energy, which means, in particular, that after a lattice block-spin transformation where $a \to sa$, one has

$$\widehat{K}'_\psi = (ag)(a\bar{\psi}\psi) \to s^2(ag)(a\bar{\psi}\psi) = s^2\widehat{K}'_\psi, \tag{3.15}$$

in contrast with (3.13). For this reason, in order to have the correct scaling, we compute the contribution to the drift without rescaling the Dirac operator (and hence the Yukawa coupling), and then rescale the whole drift via

$$\widehat{K}_\psi \to s^2\widehat{K}_\psi,$$

so that the scaling dimension of the other terms in (3.14) is matched.

We want to mention that the cooling procedure has important consequences on the issue of continuum limit of low-energy effective theories. In fact, in the standard lattice regularisation procedure, one always has $a \sim \Lambda_0^{-1}$, which means that the continuum limit $a \to 0$ is always connected to the limit $\Lambda_0 \to \infty$, in accordance to what

discussed in sections 2.1 and 2.2.

3.3.4 Control over temperature

The use of coloured noise allows one to access a wider and finer range of temperatures. In fact, as already mentioned in section 2.2, the temperature on the lattice is given by

$$T = \frac{1}{a\, N_t}. \tag{3.16}$$

Hence one can change temperature either by changing the spacing a, or by changing the number points in the time direction N_t. Both approaches pose serious constraints on the range of accessible temperatures. The spacing a is often determined by the energy scale at which one wants to simulate theory. For example in an effective theory, as explained in section 2.2, one has to keep $\Lambda \leq \Lambda_{\text{phys}}$, and since $a = \pi/\Lambda$, one ends with a constraint on the spacing $a \geq \pi/\Lambda_{\text{phys}}$.
The highest temperature reachable is then limited by mathematical arguments as one cannot have $N_t < 1$, even though in a simulation one often needs $N_t \geq 2$. On the other side the minimum temperature reachable is limited by computational resources as one cannot afford $N_t \to \infty$. Moreoveor, the resolution of high temperatures is very coarse due to the relation (3.16), in the sense that for small N_t, a change in the number of time points causes a significant variation in the temperature.

By means of coloured noise one can change the temperature by changing the effective spacing. In fact, if one follows the cooling procedure by keeping N_t fixed, one sets a new temperature which is given by

$$T_{\text{eff}} = \frac{1}{a_{\text{eff}}\, N_t} = \frac{1}{s a\, N_t} = \frac{1}{s}\, T,$$

where $s = \Lambda_{\text{eff}}/\Lambda \leq 1$. Note that not only the temperature has been raised, but one has also gained resolution around T_{eff}. In fact, to reach this temperature by changing N_t, one should change the number of time points to $N_t \to sN_t$, and for what explained before a lower N_t comes with a loss of resolution.
The control over temperature by both approaches will be investigated in section **??**. For a more detailed explanation of the procedure and its relevance in the context of the quark-meson model, we refer to [36].

3.4 Definition of relevant observables

We define the magnetisation M of the field ϕ as,

$$M = \left\langle \frac{1}{V} \sum_n \phi_n \right\rangle .$$

Thus, in a finite volume lattice system, the absolute magnetisation

$$M = \left\langle \frac{1}{V} \left| \sum_n \phi_n \right| \right\rangle .$$

is better suited as an order parameter [3, 20].
In the continumm, phase transition is characterised by a divergence in the susceptibility, or connected two-points function

$$\chi_2 = V \left(\langle M^2 \rangle - \langle M \rangle^2 \right) = V \left\langle (M - \langle M \rangle)^2 \right\rangle .$$

On a finite volume lattice, one obseres a peak that becomes sharper as the volume is increased. In pratice, the susceptibility of the order parameter

$$\chi_2 = V \left\langle (M - \langle |M| \rangle)^2 \right\rangle$$

will be adopted.
We define the fermionic two-points function

$$\begin{aligned} \langle \psi(x)\, \bar{\psi}(y) \rangle &= \frac{1}{Z} \int \mathcal{D}\phi\, \mathcal{D}\psi\, \mathcal{D}\bar{\psi}\; \psi(x)\, \bar{\psi}(y)\; \exp\left(-S_\phi - \psi D \psi + \bar{\eta}\psi + \bar{\psi}\eta\right) \\ &= \frac{1}{Z} \int \mathcal{D}\phi\, \mathcal{D}\psi\, \mathcal{D}\bar{\psi}\; \frac{\delta}{\delta \bar{\eta}(x)} \frac{\delta}{\delta \eta(y)}\; \exp\left(-S_\phi - \psi D \psi + \bar{\eta}\psi + \bar{\psi}\eta\right) \\ &= \frac{1}{Z} \int \mathcal{D}\phi\, \det\left[D(\phi)\right]\; \exp\left(-S_\phi\right)\; \frac{\delta}{\delta \bar{\eta}(x)} \frac{\delta}{\delta \eta(y)}\; \exp\left(\bar{\eta} D^{-1} \eta\right) \\ &= \left\langle \left[D^{-1}(\phi) \right]_{mn} \right\rangle . \end{aligned} \tag{3.17}$$

where D is the the Wilson-Dirac operator.
From this, the chiral condensate follows straightforwardly

$$\langle \bar{\psi}\psi \rangle = \sum_{n,s} \langle \bar{\psi}_{n,s}\, \psi_{n,s} \rangle = -\operatorname*{Tr}_{n,s} (D^{-1})_{nn}.$$

On a finite volume lattice, the correlation of a field at two spacetime points is quantified by the correlator

$$C_\psi(t,0) \equiv \frac{1}{N_x} \sum_{n_x} \left[\langle \psi(t,n_x)\, \bar{\psi}(0,0) \rangle - \langle \psi(N_t - t, n_x)\, \bar{\psi}(0,0) \rangle \right] . \tag{3.18}$$

Note that we sum up two waves because of the boundary conditions.
In momentum space, one has

$$C(t,\vec{p}) = \frac{1}{V}\sum_{\vec{x}} e^{-i\vec{p}\vec{x}} \left(\langle \Psi(t,\vec{x})\bar{\Psi}(0,\vec{0})\rangle - \left\langle \Psi\left(N_t - t,\vec{x}\right)\bar{\Psi}(0,\vec{0})\right\rangle \right)$$
$$\propto \sum_n e^{-E_n(\vec{p})t} - e^{-E_n(\vec{p})(N_t-t)} = \sum_n 2e^{-E_n(\vec{p})\frac{N_t}{2}} \sinh\left[E_n(\vec{p})\left(\frac{N_t}{2} - t\right)\right].$$

For large times all the contributions but the ground state are suppressed, so that the fermionic correlator assumes the form

$$C_\psi(t,0) \approx \sinh\left(E_0^\psi\left(\frac{N_t}{2} - t\right)\right), \tag{3.19}$$

where E_0^ψ is the fermionic mass gap, which will be denoted as $m_{q,\text{phys}}$.
Hence by computing the correlator on the lattice by means of (3.17), one can measure fermionic masses in the simulation by making a fit to expression (3.19).

Chapter 4

Numerical results: preliminaries

4.1 Inversion of the Dirac operator

As mentioned in section 3.2, the inversion of the Dirac operator is a computationally expensive operation. In fact, simple algorithms to invert a matrix such as Gaussian elimination have computational complexity of $O(n^3)$ [37], while the best algorithm available nowadays has been proved to scale as $O(n^{2.371552})$ [32].
To circumvent this, since we are often only interested in applying the inverse matrix to a vector, we make use of the Conjugate Gradient algorithm, as detailed in appendix C.
We now want to give an idea of the speed-up that one can gain by following such approach, keeping in mind that this is an operation which has to be performed at each evolution step.
To do this, we construct a Dirac operator described by equation (3.4) with bare quark mass $m_q = 0.5$ and Yukawa coupling $g = 0.5$. We then add a fluctuating scalar field

$$\phi(x) = v + \eta(x),$$

where $v = 1.0$ and η is a normally distributed number with mean 0 and unitary variance.
We then measure the time needed to compute

$$\xi = D^{-1}\psi,$$

where ψ is a vector of random numbers uniformly ditributed between -1 and 1. We study the time dependence as a function of the vector size V by averaging over 20 measures per each value of V.
Figure 4.1 reports the results of the experiment. Assuming that our algorithm has complexity $O(V^b)$, namely that when $V \to \infty$

$$t \approx a\, V^b,$$

we fit our data according to the model

$$\log t = \log a + b \log V.$$

We find

$$\log a = -3.1 \pm 0.1 \qquad b = 1.02 \pm 0.02.$$

Note that for a standard Gaussian elimination procedure we would have found $b \approx 3.0$. This is of particular relevance in the case of this work, since the cooling technique via coloured noise requires doubling the number of lattice points in each direction at each block spin step; hence the volume of the lattice increases by a factor

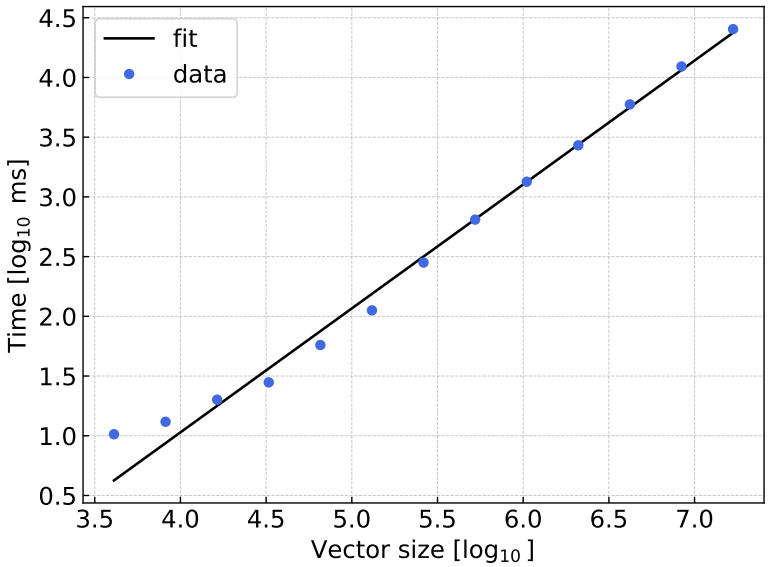

FIGURE 4.1: Computational complexity of the Conjugate Gradient algorithm in our model. The results show the operation time scales as $t \sim \mathcal{O}(V^{1.03})$ for large verctor sizes, while for a standard Gaussian elimination one would have found $t \sim \mathcal{O}(V^3)$.

2^d at each iteration, where d is the spacetime dimension.
Typical lattices sizes in this work are up to $128 \times 128 \times N_f \times N_s \approx 10^5$, where N_f is the number of flavours and N_s is the number of spinor components. Therefore, a good volume scaling of the algorithm is strictly necessary.

4.2 The fermionic correlator

We now want to analyse the behaviour of the fermionic correlator and illustrate the fermionic masses extraction procedure.
Let us for the moment restrict to $g = 0$, so that the Dirac operator reduces to the one of free Wilson fermions

$$\begin{aligned}\widehat{D}_{m,n} = &- \left(\frac{\Gamma_{+\hat{0}}}{2}\,\delta_{m,m+\hat{0}} + \frac{\Gamma_{-\hat{0}}}{2}\,\delta_{m,m-\hat{0}} + \frac{\Gamma_{+\hat{1}}}{2}\,\delta_{m,m+\hat{1}} + \frac{\Gamma_{-\hat{1}}}{2}\,\delta_{m,m-\hat{1}} \right) \\ &+ (2ar + \hat{m})\;\delta_{s,s'}\,\delta_{m,n}.\end{aligned} \tag{4.1}$$

We then compute the correlator (3.18) numerically via a single inversion of the Dirac operator using the Conjugate Gradient algorithm as detailed in Appendix C. The lattice volume is chosen to be 128×128.

Figure 4.2 reports the fermionic correlator as a function of m_q. One can see that a bigger bare quark mass results in a quicker decay, according to the decay law

$$\lim_{t\to\infty} \langle \psi(t)\bar{\psi}(t)\rangle_{s,s'} \propto e^{-m_{\text{phys}}\,t}.$$

On the other side, a smaller mass results in a slower decay and tends to deform the characteristic shape of the correlator.

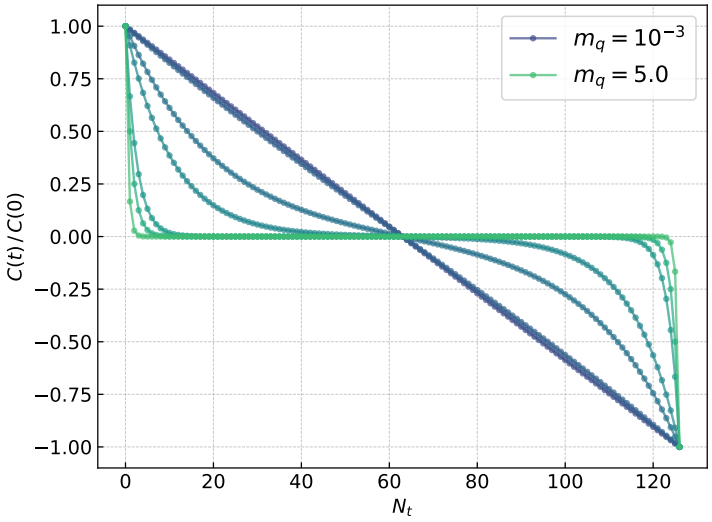

FIGURE 4.2: Normalised fermionic correlator for different values of the bare quark mass.

Figure 4.3 shows the number of iterations needed for convergence of the Conjugate Gradient algorithm. While the exact number depends on the desired tolerance, one can clearly see that the number of iterations grows as $m_q \to 0$, due to an increase in the condition number [37].

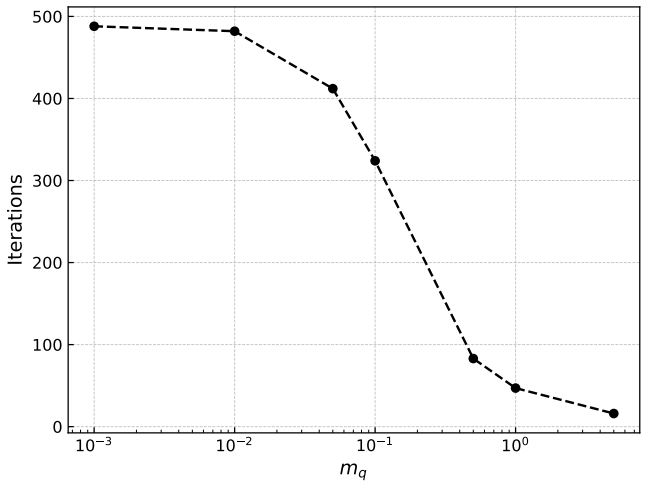

FIGURE 4.3: Conjugate Gradient algorithm iterations as a function of the bare quark mass.

For the Dirac operator 4.1, one can derive an analytical expression for the physical mass, the pole of the propagator.
To do this, let us consider the momentum space expression of the Dirac operator, which is derived in appendix B

$$\bar{D}(p) = \hat{m}_q + \sum_\mu 2\sin^2\left(\frac{p_\mu a}{2}\right) + i\sum_\mu \gamma_\mu \sin\left(p_\mu a\right).$$

This can be straightforwardly inverted to

$$\bar{D}^{-1}(p) = \frac{\hat{m}_q + \sum_\mu 2\sin^2\left(\frac{p_\mu a}{2}\right) - i\sum_\mu \gamma_\mu \sin\left(p_\mu a\right)}{\hat{m}_q + \sum_\mu 2\sin^2\left(\frac{p_\mu a}{2}\right) + \sum_\mu \sin^2\left(p_\mu a\right)}.$$

One can now find the pole by imposing the numerator evaluated at $p^\mu = (im_{\text{phys}}, 0)$ to zero:

$$\left[\hat{m}_q + \sum_\mu 2\sin^2\left(\frac{p_\mu a}{2}\right)\right]^2_{p_\mu=(im_{\text{phys}},0)} + \left[\sum_\mu \gamma_\mu \sin\left(p_\mu a\right)\right]^2_{p_\mu=(im_{\text{phys}},0)} = 0.$$

This results in a trascendental equation

$$\left[\hat{m}_q - 2\sinh^2\left(\frac{\hat{m}_{\text{phys}}}{2}\right)\right]^2 - \sinh^2\left(\hat{m}_{\text{phys}}\right) = 0,$$

which has the solution

$$\hat{m}_{\text{phys}} = \log\left(1 + \hat{m}_q\right). \tag{4.2}$$

We then choose three values of the bare quark mass, compute the correlator numerically and perform a fit according to (3.19), in order to extract the physical mass. We then compare it to the theoretical value given by (4.2). The results are reported in figures 4.4 and table 4.1.

Note that in an interacting theory, excited states are, strictly speaking, negligible only for $t \to \infty$. This means that they may affect the characteristic shape of the correlator, and one has to either consider only a smaller window centered around $t = N/2$, or to fit the two exponential decays separately, in order to extract the mass I might try to bring an example.

m_q	teo	fit
1.0	0.6931471805599453	0.6931537171644739
0.1	0.09531017980432493	0.09531020915059212
0.01	0.009950330853168092	0.009950277657505842

TABLE 4.1: The correlator for free Wilson fermions is fitted to equation (3.19) and compared to its analytical value given by (4.2). The precision for the Conjugate Gradient algorithm was set to $r^2 \leq 10^{-10}$.

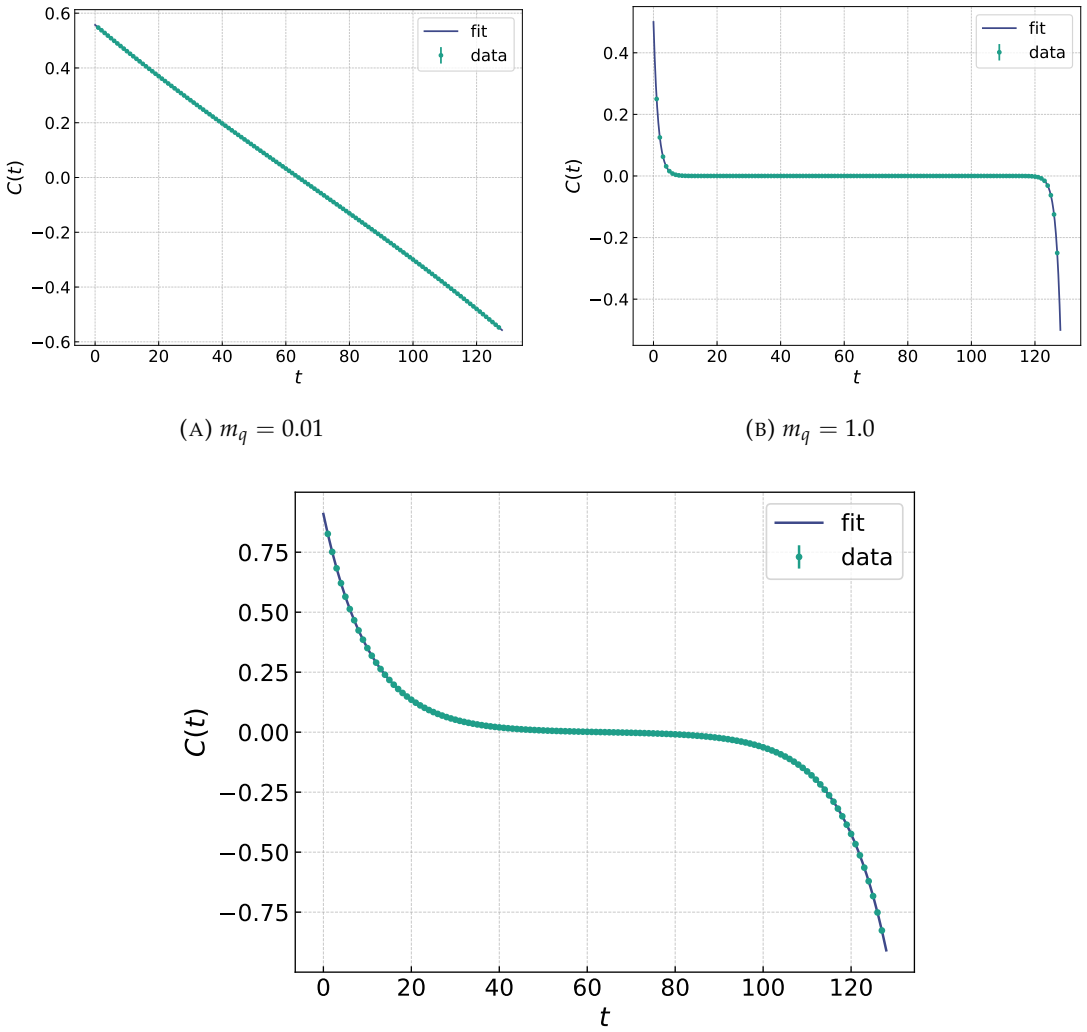

(A) $m_q = 0.01$

(B) $m_q = 1.0$

(C) $m_q = 0.1$

FIGURE 4.4: Fit of the fermionic correlator acording to equation (3.19), for three different values of the bare quark mass.

4.3 Phase structure

We want to start the analysis of the Yukawa theory by doing a parameters scan, in order to have a global picture of the phase diagram in the presence of Wilson fermions. For the remaining of this section, we set the value of the fermionic bare mass to $m_q = 1.0$.

Figure 4.5 reports a slice of the phase diagram in the $g - m_\phi^2$ plane.
For $g = 0$, the fermionic and bosonic theories are independent. In particular the scalar theory reduces to a O(1) interacting theory: for $m_\phi^2 > 0$ the systems lies in a symmetric state identified by $\langle \phi \rangle = 0$. As the mass goes to negative values, the scalar field gains a non-zero expectation value, signaling the spontaneous breaking of the O(1) symmetry.
When a finite Yukawa coupling is added, the finite bare quark mass and the Wilson term, that break chiral symmetry explicitly, are fed to the scalar field, which gains a vacuum expectation value due to the relation (2.25).
Note that the diagram of the magnetisation is in good agreement with the qualitative description of the phase structure given in section 2.5.

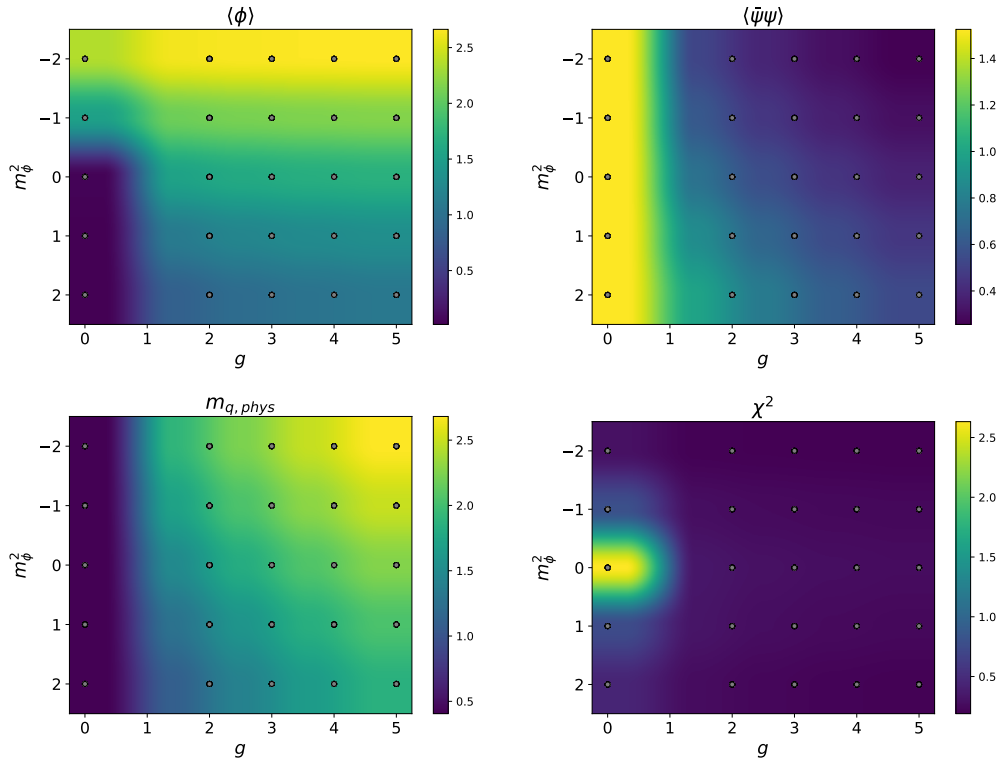

FIGURE 4.5: Slice of the phase diagram at fixed $\lambda = 2.0$.
Lattice size 32×32, $N_{\text{conf}} \approx \mathcal{O}(5 \cdot 10^4)$.

The plot of the chiral condensate shows that chiral symmetry is always broken in the model, even for $g = 0$. Because of this, even for finite m_q and g one can never speak of a proper phase transition. Thus, one still have a smooth crossover between the two phases. This fact is reflected in the plot of the magnetic susceptibility, which peaks around $m_\phi^2 = 0$ only for small values of g.
As explained in section 2.5, the presence of a background scalar field can be interpreted as a bare quark mass. This is reflected in the plot of of $m_{q,\text{phys}}$ which

resembles the one of $\langle\phi\rangle$, except for $g = 0$, where the two theories are disconnected.

Figure 4.6 reports the phase diagram in the $\lambda - g$ plane. The behavior can be understood qualitatively by means of classical arguments. For $g = 0$, one expects a field magnetisation of order

$$v = \sqrt{-\frac{6m_\phi^2}{\lambda}}.$$

Hence, as λ is increased, the expectation value of the field is reduced. If $g \neq 0$, the fermion masses contributions increase the expectation value of the field, which in turn works as an additional bare quark mass, hence increasing $m_{q,\text{phys}}$. The behavior of the susceptibility is analogous to the previous case: only if $g = 0$ one has a proper phase transition, reflected in the single peak. The precise value of λ at which this happens, depends, mainly, on the choice of m_ϕ^2. potrei anche fare un plot a $m_\phi^2 > 0$

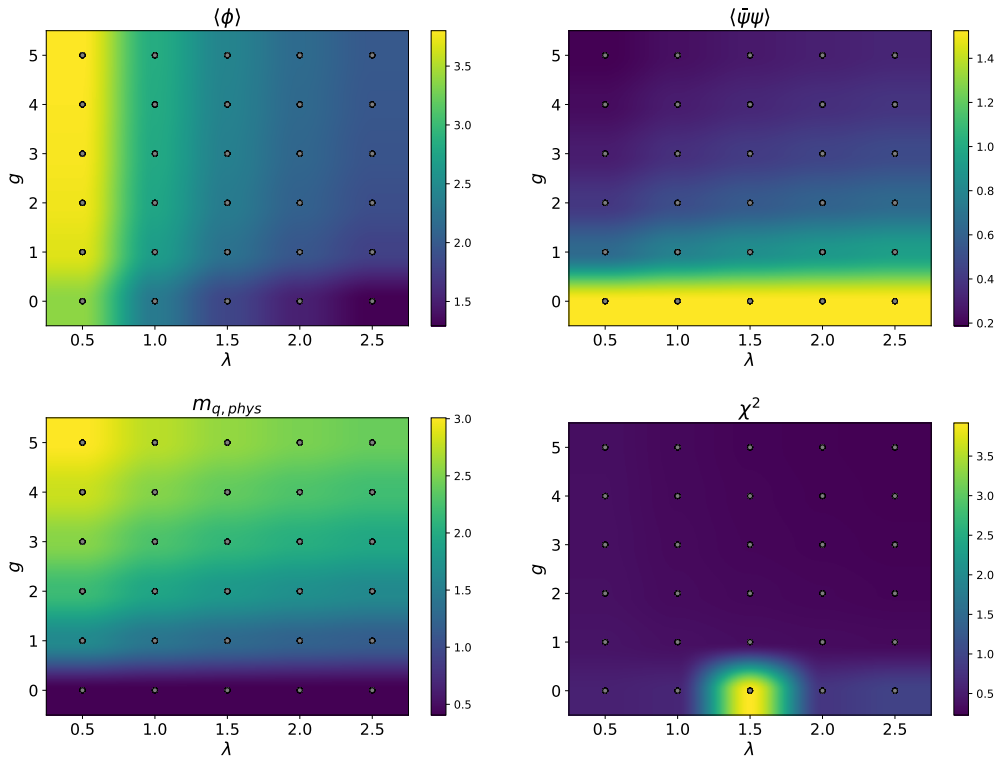

FIGURE 4.6: Slice of the phase diagram at fixed $m_\phi^2 = -1.0$.
Lattice size 32×32, $N_{\text{conf}} \approx \mathcal{O}(10^4)$.

Finally, let us give a look at the phase structure in the $\lambda - m_\phi^2$ plane. Since here one always has $g \neq 0$, the expectation value of the scalar field and the chiral condensate are never zero, since the symmetry is broken independetly of the choice of m_ϕ^2 and *lambda*. This fact is also reflected in the mass plot, where one can clearly see that m_{phys} is always proportional to the field.

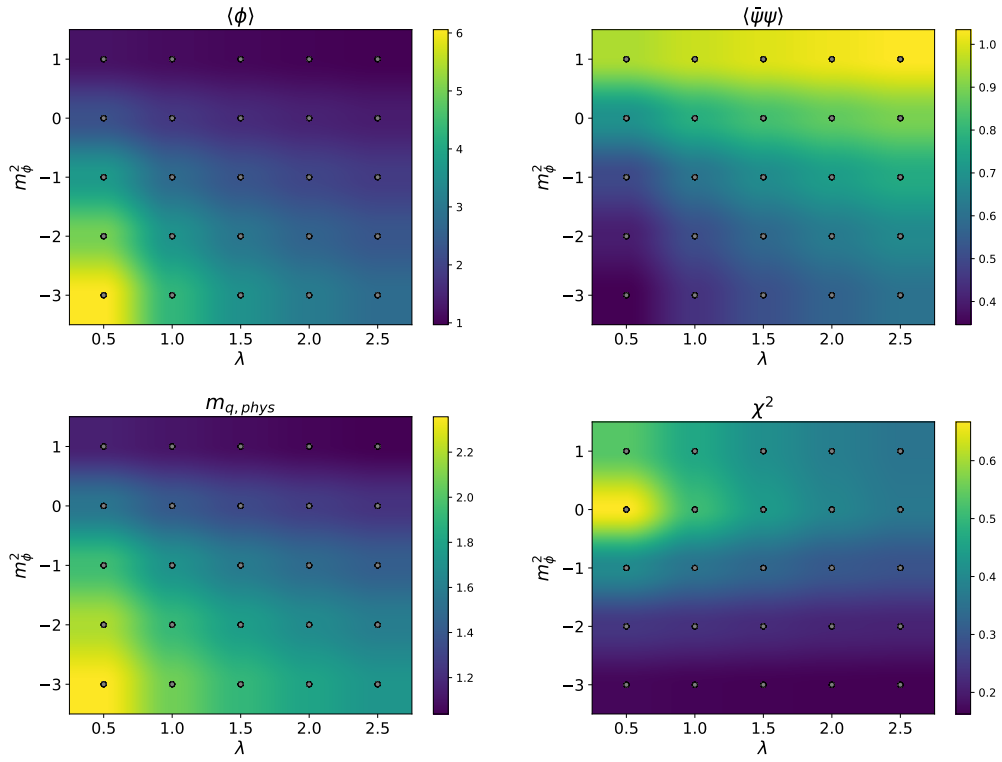

FIGURE 4.7: Slice of the phase diagram at fixed $g = 1.5$.
Lattice size 64×64, $N_{\text{conf}} \approx \mathcal{O}(10^4)$.

Moreover, the susceptibility in this case does not show a single peak as the phase transition can only happen for $g = 0$. Note in fact the difference in magnitude with respect to figures 4.5 and 4.6.

Chapter 5

Numerical results: coloured noise

5.1 Classical-to-quantum interpolation

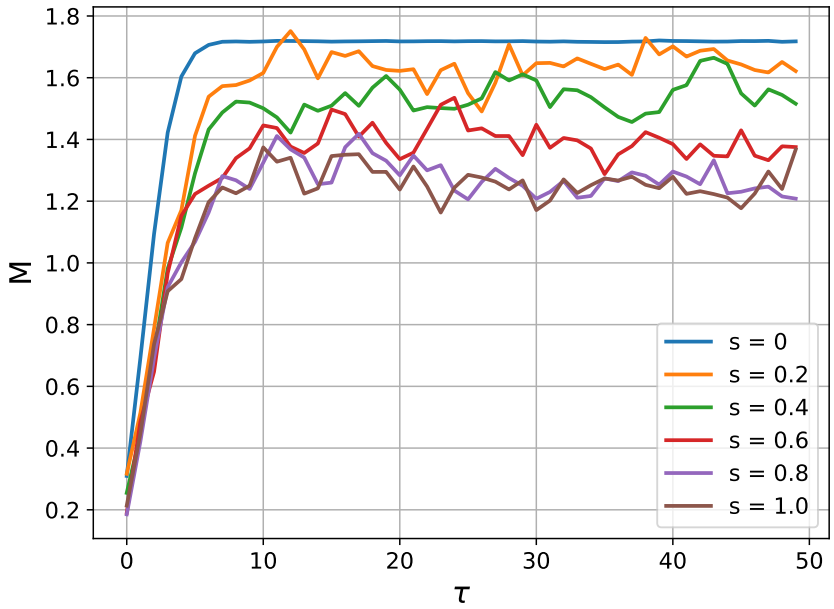

FIGURE 5.1: Thermalisation of the system for different values of the noise fraction s. As noise is added, the equilibrium state of the system shifts accordingly. Coloured noise allows for a smooth interpolation between the fully classical and fully quantum picture.
Lattice size 32×32, $m_\phi^2 = -1.0$, $\lambda = 0.5$, $g = 0.08$, $m_q = 0.5$.

Let us start by analising the coloured noise field in the simulation and relevant properties that emerge from it. We consider the Yukawa model described by the continuum action (2.16) and its discrete version (3.5), (3.6).
The system is initialised in the same state for all the configurations on a 64×64 lattice. We consider a simulation with $s = 1$ and then progressively lower the cutoff fraction s, keeping fixed all the quantities in the classical action.
Figure 5.1 shows the system thermalisation for different values of s, namely the Langevin evolution from the initial state to equilibrium. The blue line corresponds to the case $s = 0$, a classical simulation, while the brown line corresponds to the case $s = 1$, the fully quantum case. All the parameters settings are reported under the figure.
One can notice that as quantum modes are removed via coloured noise, the systems shifts its equilibrium point.

We now want to make use of coloured noise to understand the relation between scalar field, quark condensate and fermionic mass, which was qualitatively discussed in section 2.5 by means of classical arguments.
Keeping all the parameters fixed, we perform simulations changing the value of the cutoff fraction s, and we measure the three quantities above mentioned: the results are reported in figure 5.2. One can clearly see that as quantum modes are added, the relation between the three quantities

$$\langle \phi \rangle \sim \langle \bar{\psi}\psi \rangle \sim m_q.$$

change proportionally.

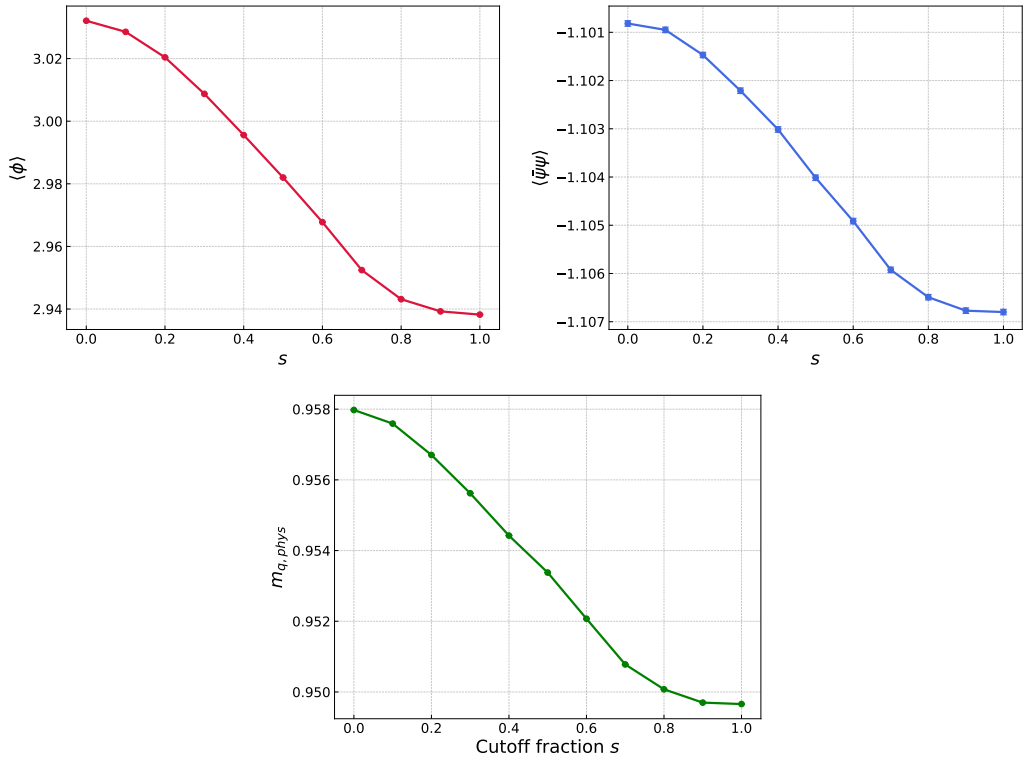

FIGURE 5.2: x label Relation between magnetisation, chiral condensate and mass, which was motivated in section 2.5.
$m_\phi^2 = -1.0,\ \lambda = 0.7, g = 0.2,\ m_q = 1.0$
Lattice size 64×64, $N_{\text{conf}} \approx \mathcal{O}(5 \cdot 10^4)$.

This makes clear at first that the scalar field ϕ effectively plays the role of quark bilinear in the dynamics. Moreoveor, the presence of a background field generates a quark, which breaks chiral symmetry.
The interconnection of these phenomena is an important result if one interprets it in the context of effective theories. In fact, often in QCD, the dynamical chiral symmetry breaking mechanism is described by low energy Yukawa-type effective models such as Gross-Neveu, Nambu - Jona-Lasinio or Quark Meson, to name some examples, where a scalar field can emerge after bosonisation via a Hubbard-Stratonovich transformation, as mentioned in chapter 1.
Beeing low-energy effective theories, one expects them to hold only up to a certain eenrgy scale, typically menziona. Since via coloured noise the cutoff can be

controlled, as discussed in where, knowint that the relation holds at all level is of high relevance.
For $s = 0$, the fields are restricted to the classical equations of motion (2.21). As pointed out in section 2.5, in particular in equation (2.24), a background field $\phi(x) = v$ has the same behaviour on the system as a bare quark mass. We then compare the physical quark mass with the theoretical expression for free Wilson fermions (4.2) using a shifted bare mass

$$M_q = m_q + g \langle \phi \rangle$$

The comparison is reported in table 5.1

m_q	g	$\langle \phi \rangle$	M_q	$\log(1 + M_q)$	m_{phys}
1.0	0.2	3.032082758	1.606416551	0.957976309	0.957976383

TABLE 5.1: The physical quark mass of the classical system is compared with the theoretical result for Wilson fermions, using the shifted bare mass $M_q = m_q + g \langle \phi \rangle$. This shows that a background scalar field can be interpreted as a bare quark mass.

5.2 Chiral fermions and noise-induced transition

As explained in section 2.5, chiral symmetry can be broken, in the continumm theory, either explicitly via the introduction of a finite bare quark mass, or spontaneously if the field gains a non-zero expectation value.
Moreoveor, in the discrete formulation, the introduction of the Wilson term contributes to the explicit breaking of chiral symmetry, as shown in appendix B. This, in particular, means that chiral symmetry is explicitly broken also for $m_q \to 0$. Because of this, one needs a new definition of the bare mass M_q, which takes into account the Wilson term contribution, such that chiral symmetry is restored in the limit $M_q \to 0$.
In a lattice study of a theory suchs as two-flavours QCD, what one typically does [2, 3] is the following: the spontaneous breaking of chiral symmetry generates three goldstone massless bosons, the pions. If the bare quark mass is zero, the physical mass of the pions has to be zero, as a consequence of Goldstone's theorem [38]. Hence one can measure the pions mass and find a value m_q^* such that when $m_q \to m_q^*$ one has $M_\pi \to 0$.
This approach is not feasible in our theory, since it is described by a discrete chiral symmetry.
In the literature, one can find proposals for the definition of a bare quark mass for similar theories [39, 40]. Thus such approaches are not followed here, both because of time reasons, but also because it is not our purpose to match any precise model, but rather investigate properties of the coloured noise technique. Hence, here we just consider naïve fermions and the chiral limit is reached for $m_q \to 0$. Thus, one has to keep in mind that due to the fermion doubling this represents a theory with $2N_f = 4$ degenerate quarks.

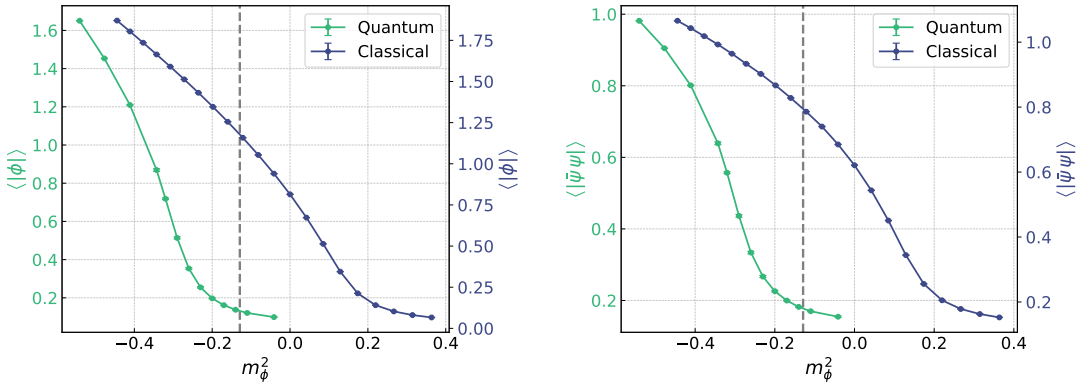

FIGURE 5.3: Mass scan of the quantum and classical theories. The dashed gray line indicates a value $m_\phi^{2,*}$, where the classical and quantum systems lie in two different phases.

In figure 5.3, the (absolute) magnetisation and the chiral condensate are studied as a function of the bosonic mass squared, both in the fully quantum and fully classical theory. One can notice that the classical system undergoes a phase transition at values of m_ϕ^2 bigger than the quantum counterpart. Note that as the bare quark mass is small but finite, this is not a proper phase transition and the latter will be, eventually, reached in the limit $m_q \to 0$. We then pick a value $m_\phi^{2*} = -0.123$ which is represented by a gray line in figure 5.3.

Using coloured noise, we then interpolate between the classical and quantum picture for different values of the quark mass, namely $m_q = 10^{-2}, 5 \cdot 10^{-3}, 10^{-3}$.

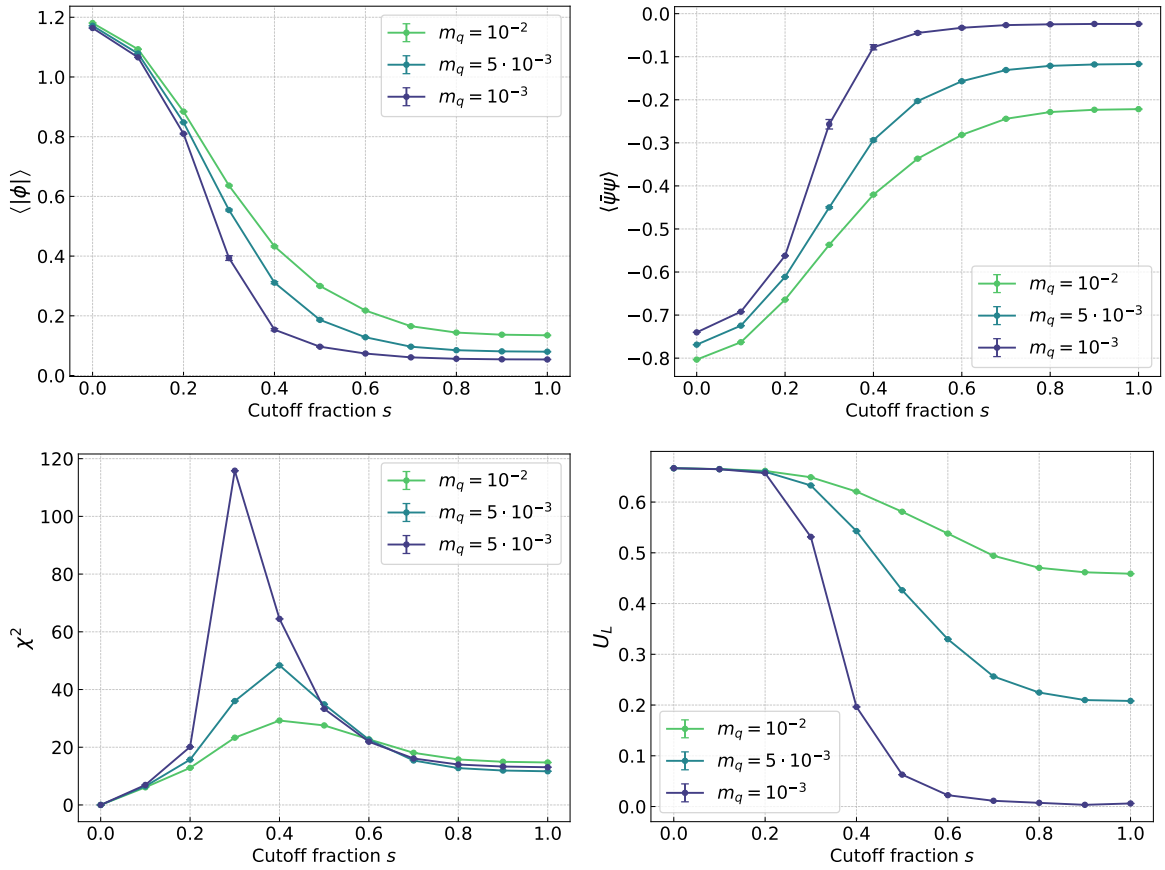

FIGURE 5.4: $m_\phi^2 = -0.123,\ \lambda = 1.951, g = 0.08,$
Lattice size $64 \times 64,\ N_{\text{conf}} \approx \mathcal{O}(5 \cdot 10^4)$

One can clearly see in figure 5.4 that as the quark mass is lowered the difference between the two phases gets sharper, indicating a phase transition. This is especially highligthed in the increasing peak of the magnetic susceptibility, and by the Binder parameters, which assumes the value $U_L = 0$ in the symmetric phase, and $U_L = 2/3$ in the broken phase.
Note that in order to confirm that a phase transition took place, one should first consider $V \to \infty$ and then $m_q \to 0$. If the order parameters of the classical and quantum theories still indicates that the system is in two different phases, one can draw the conclusion.

5.3 Cooling with coloured noise

Let us now consider one of the main applications of coloured noise, namely the cooling technique.
We first set up a white noise simulation $s = 1$, and then progressively lower s. The lowering of the cutoff is compensated by a change in the couplings, as explained in section 3.3. We study the behavior of the system both as a function of the bosonic mass squared m_ϕ^2 and the Yukawa coupling g. A summary of the parameters choice for both the experiments is reported in tables 5.2 and 5.3.

s	N_t	N_x	m_ϕ^2	λ	g	m_q	K_ψ
1	16	16	m_ϕ^2	0.4	0.3	0.5	K_ψ
1/2	32	32	$m_\phi^2/4$	0.1	0.3	0.5	$K_\psi/4$
1/4	64	64	$m_\phi^2/16$	0.025	0.3	0.5	$K_\psi/16$
1/8	128	128	$m_\phi^2/64$	0.00625	0.3	0.5	$K_\psi/64$

TABLE 5.2: Parameter settings in the cooling procedure for the bosonic mass squared scan. Each coupling in the bosonic action is rescaled according to its canonical dimension, while the fermionic sector rescaling is implemented directly at the drift level, as detailed in section 3.3

.

s	N_t	N_x	m_ϕ^2	λ	g	m_q	K_ψ
1	16	16	0.5	0.7	g	1.0	K_ψ
1/2	32	32	0.125	0.175	g	1.0	$K_\psi/4$
1/4	64	64	0.0625	0.04375	g	1.0	$K_\psi/16$
1/8	128	128	0.03125	0.001094	g	1.0	$K_\psi/64$

TABLE 5.3: Parameters setting in the cooling procedure for the Yukawa coupling scan. Each coupling in the bosonic action is rescaled according to its canonical dimension, while the fermionic sector rescaling is implemented directly at the drift level, as detailed in section 3.3

.

Figure 5.5 reports the magnetisation, its susceptibility and the chiral condensate as a function of the bare scalar mass squared m_ϕ^2, while figure 5.6 reports the investigation as a function of the Yukawa coupling.
One can clearly see that there is a general good agreement for the first three block-spin transformations, even if based on tree level arguments.

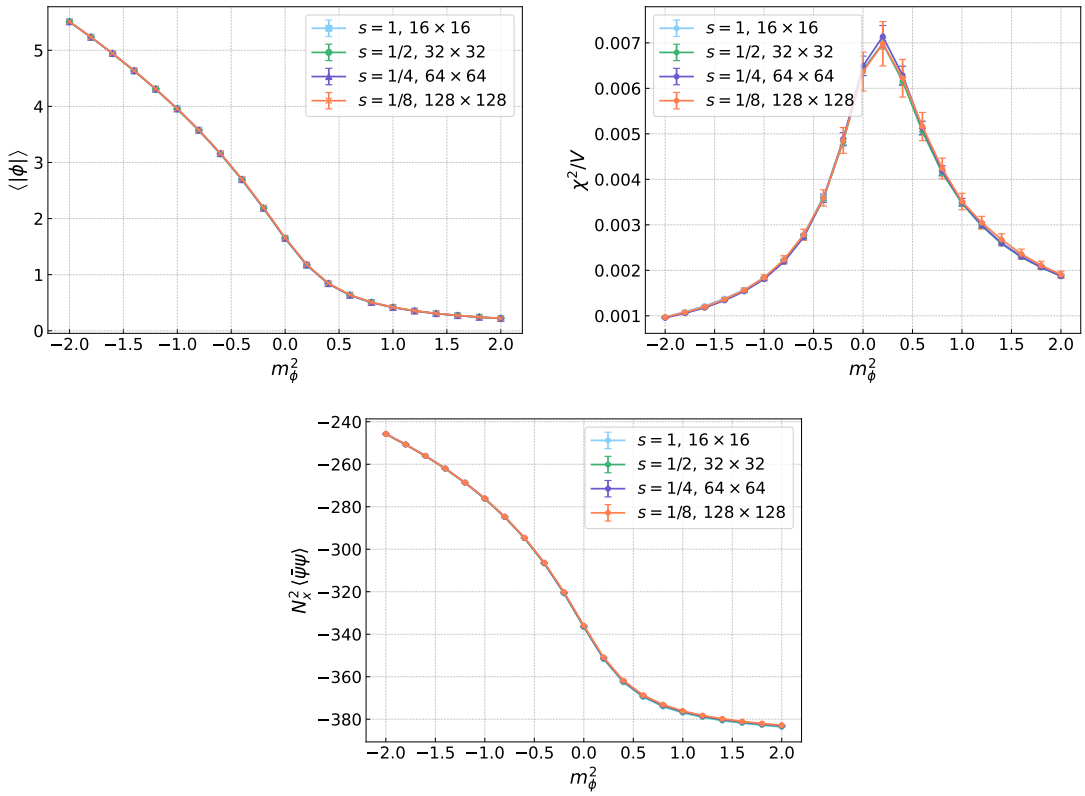

FIGURE 5.5: Cooling via coloured noise. The absolute magnetisation, its susceptibility and the chiral condensate are compared after performing block-spins transformations as a function of the bosonic mass squared.
$N_{\text{conf}} \approx \mathcal{O}(5 \cdot 10^4)$. The other parameters are reported in table 5.2

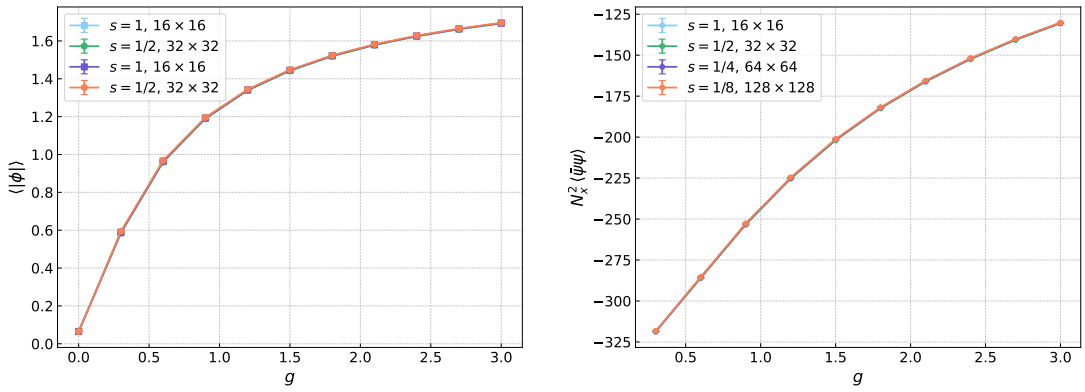

FIGURE 5.6: Cooling via coloured noise. The absolute magnetisation and the chiral condensate are compared after performing block-spins transformations as a function of the Yukawa coupling.
$N_{\text{conf}} \approx \mathcal{O}(5 \cdot 10^4)$. The other parameters are reported in table 5.3.

The most relevant observables are the magnetisation and the chiral condensate, since they are the order parameters of the theory. We therefore want to provide a more detailed comparison of the performance of the procedure. To this end we define the relative errors

$$\begin{aligned} \epsilon_\phi(s) &= \frac{\langle |M| \rangle_s - \langle |M| \rangle}{\langle |M| \rangle}, \\ \epsilon_\psi(s) &= \frac{\left\langle |\bar{\hat{\psi}}\, \hat{\psi}| \right\rangle_s - \left\langle |\bar{\hat{\psi}}\, \hat{\psi}| \right\rangle}{\left\langle |\bar{\hat{\psi}}\, \hat{\psi}| \right\rangle}. \end{aligned} \tag{5.1}$$

The deviation quantified by such parameters is reported in figures 5.7 and 5.8.

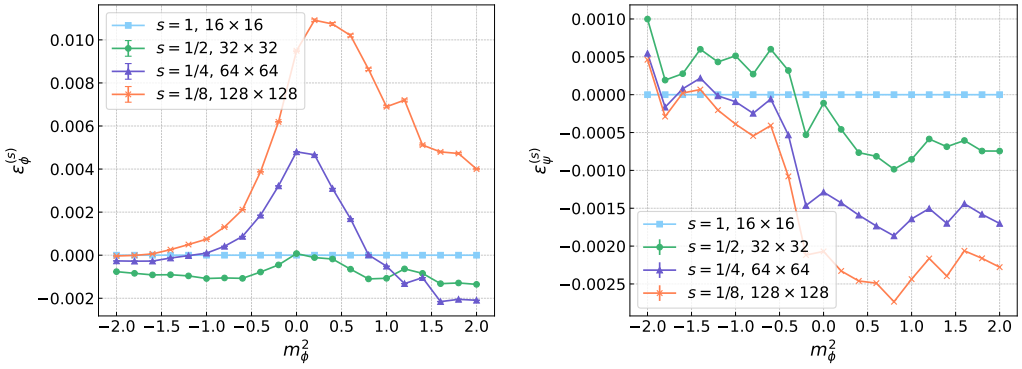

(A) Absolute magnetisation (B) Chiral condensate

FIGURE 5.7: Relative error of the absolute magnetisation and chiral condensate in the cooling procedure for various values of the noise fraction s.

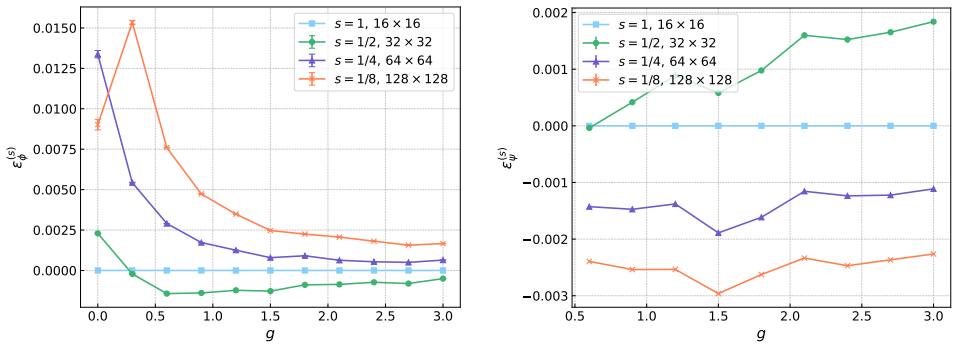

(A) Absolute magnetisation (B) Chiral condensate

FIGURE 5.8: Relative error of the absolute magnetisation and chiral condensate in the cooling procedure for various values of the noise fraction s.

Finally, we also want to look at more complex observables such as the fermionic physical mass and the bosonic renormalised mass. They are reported in figure 5.9. As one can see, there is a clear deviation for $m_{\phi,r}$ at the third block-spin iteration.

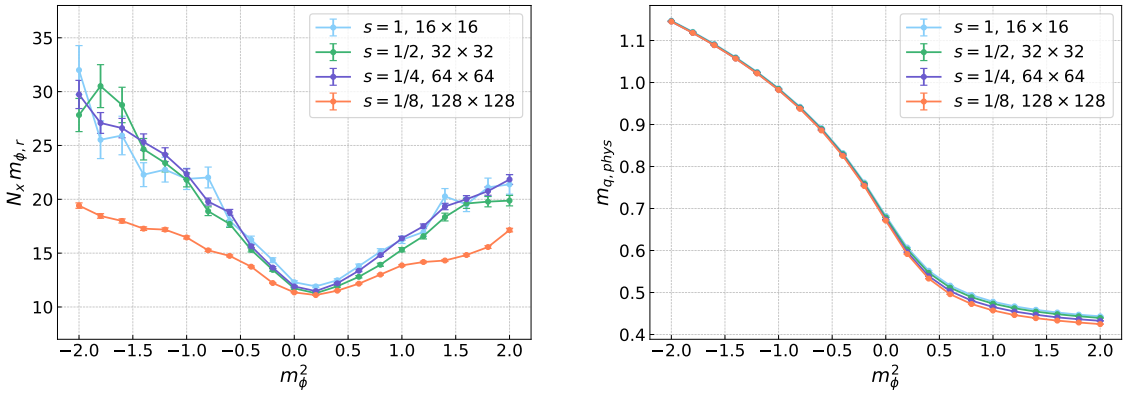

FIGURE 5.9: Renormalised bosonic mass $m_{\phi,r}$ and pole fermionic mass $m_{q,\text{phys}}$ for various values of the noise fraction s.

We now want to comment on the results obtained and motivate discrepancies, when possible. Errors obviously increase with successive iterations, since the approximations are multiple.
First of all, a tree level rescaling neglects coupling momentum dependencies which do not stem from spacetime rescaling; the assumption is thus justified for high enough cutoffs.
Moreover, the assumption that any change due to a modification of the cutoff can be absorbed by a redefinition of the couplings, is itself non-trivial. In fact, following Wilsonian's RG perspective, as momentum shells are integrated out, all relevant operators grow as the cutoff is lowered and, if not present in the action, have to be taken into account. As before, the assumption is justified for high enough cutoffs. A quantitative analysis in this sense was done in [24], where it was proposed a procedure to systematically test untill when it is possible to accomodate the cutoff change by a redefinition of the couplings, eventually including also beyond tree level transformations.
Another delicate issue resides in the use of sharp cutoffs to regulate the noise term. In fact, as shown in section 2.3.2, the noise-to-noise correlation function expressed in momentum space exhibits an oscillating behaviour described by a Bessel function, which was calculated and shown in figure 2.2.
As a consequence, correlation functions are affected by this behaviour. This holds particularly for the connecte two-points function as shown in figure 5.10. This explains the big discrepancy encountered in the renormalised mass in figures 5.9 and other plot, when added. In any case, this error cannot be solved by simply going to higher order correction to the rescaling procedure, but can only be fixed by changing the regulating term, since it is an intrinsic characteristic of the latter. Possible alternative regulators are discusses in [24]. For what concerns the physical quark mass, which also shows some discrepancy for $m_\phi^2 > 0$, we did not investigated further the source of error.
Finally, since the regulating term applies strictly speaking, only to the noise term, after performing a block-spin transformation the quantum theory is set back at its original scale, while the classical one lies at double the spacing, which is now coarser.

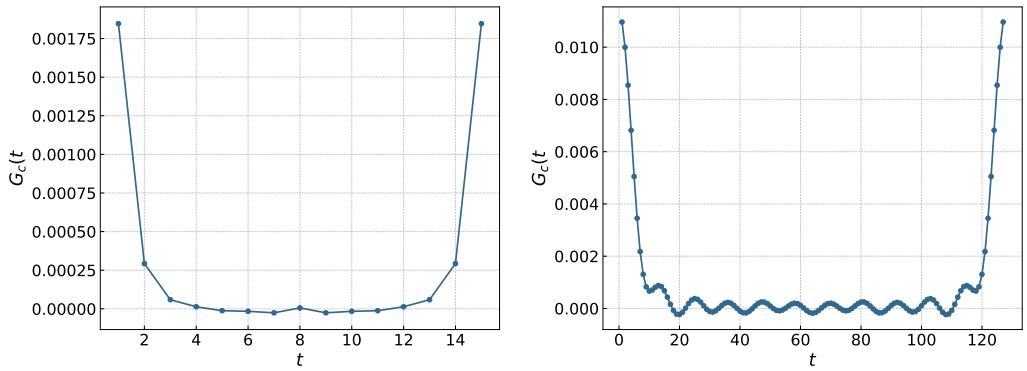

FIGURE 5.10: (Left) Connecte two-points function of the original theory on the 16×16 lattice. (Right) Connected two-points function after three block spin-iterations at cutoff fraction $s = 1/4$. The use of the sharp cutoff as a regulating function results in a disturbance of the signal of the bosonic two-points function. Bessel function profile which was shown in figure 2.2. This induces errors in the calculation of the effective mass.

It is nevertheless remarkable that observables such as the order parameters are not significantly altered in the coarse-graining procedure,

Chapter 6

Conclusions and outlook

Appendix A

Conventions

Spinor representation

We choose the following representation of the two-dimensional γ matrices

$$\gamma_0 = \sigma_3 = \begin{pmatrix} 1 & 0 \\ 0 & -1 \end{pmatrix} \qquad \gamma_1 = \sigma_1 = \begin{pmatrix} 0 & 1 \\ 1 & 0 \end{pmatrix}$$

They satisfy the Euclidean Clifford algebra

$$\{\gamma_\mu, \gamma_\nu\} = 2\delta_{\mu,\nu}$$

and they have the following properties

$$\gamma_\mu^\dagger = \gamma_\mu, \qquad \gamma_\mu^2 = \mathbb{1}.$$

We then introduce γ_5 as

$$\gamma_5 = i\gamma_0\gamma_1 = \begin{pmatrix} 0 & i \\ -i & 0. \end{pmatrix}$$

with the following properties

$$\gamma_5^\dagger = \gamma_5, \qquad \gamma_5^2 = \mathbb{1} \quad (\gamma^5)^2 = \mathbb{1}, \qquad \{\gamma_5, \gamma_\mu\} = 0$$

Fourier transform

The Fourier transformation of a function $f : \mathbb{R}^d \to \mathbb{R}$ is given by

$$\bar{f}(p) = \mathcal{F}[f](p) = \int_x e^{-ixp} f(x)$$

and its inverse is

$$f(x) = \mathcal{F}^{-1}[\bar{f}](x) = \frac{1}{(2\pi)^d} \int_p e^{ixp} \bar{f}(p)$$

Appendix B

Wilson fermions

The naïve discretisation of the fermionic action for free fermions yields the Dirac operator components

$$\widehat{D}_{nm} = \sum_{\mu} \gamma_\mu \, \frac{\delta_{n,n+\mu} - \delta_{n,n-\mu}}{2} + m_q \delta_{n,m},$$

which have the momentum representation

$$\widehat{D} = \hat{m}_q + i \sum_{\mu} \gamma_\mu \sin\left(p_\mu \, a\right).$$

The last expression can be easily inverted

$$\widehat{D}^{-1}(p) = \frac{\hat{m}_q - i \sum_\mu \gamma_\mu \sin\left(p_\mu \, a\right)}{\hat{m}_q^2 + \sum_\mu \sin^2\left(p_\mu \, a\right)}.$$

For $m_q = 0$, one can easily see that, in addition to $\hat{p}_\mu = 0$, all the edges of the Brillouin zone $\hat{p}_\mu \in \{\pm\pi/a, \pm\pi/a\}$ are poles. They indeed represent additional fermions, which come from the discretisation of the action. These additional degrees of freedom are called doublers and represent unphysical particles, at least if one's goal is to recover the original continuum theory. If m_q is finite,
The idea proposed by Wilson to remove the doublers is to redefine the action as

$$S_W = S - \frac{r}{2} \sum_{m,n} \hat{\bar{\psi}}(m) \, \hat{\Box} \, \hat{\psi}(n),$$

where

$$\left(\hat{\Box}\right)_{mn} = \sum_{\mu} \frac{\delta_{m,n+\hat{\mu}} + \delta_{m,n-\hat{\mu}} - 2\,\delta_{mn}}{2},$$

and $r \in [0, 1]$ is a free parameter. In this project we always consider $r = 1$.
The Wilson-Dirac operator assumes the form

$$\widehat{D} = \hat{m}_q + \sum_{\mu} \gamma_\mu \frac{\delta_{m,m+\hat{\mu}} - \delta_{m,m-\hat{\mu}}}{2} + \frac{r}{2} \sum_{\mu} \frac{\delta_{m,n+\hat{\mu}} + \delta_{m,n-\hat{\mu}} - 2\,\delta_{mn}}{2}.$$

and its momentum space representation is

$$\begin{aligned}\widehat{D}(p) &= \hat{m}_q + i\sum_\mu \gamma_\mu \sin\left(p_\mu a\right) + \frac{r}{2}\sum_\mu \left[\cos\left(p_\mu a\right) - 1\right] \\ &= \hat{m}_q + i\sum_\mu \gamma_\mu \sin\left(p_\mu a\right) + r\sum_\mu \frac{\cos\left(p_\mu a\right) - 1}{2} \\ &= \hat{m}_q + i\sum_\mu \gamma_\mu \sin\left(p_\mu a\right) + r\sum_\mu \sin^2\left(\frac{p_\mu a}{2}\right).\end{aligned}$$

The last expression can be inverted straightforwardly

$$\begin{aligned}\widehat{D}^{-1}(p) &= \frac{\hat{m}_q + \frac{2r}{a}\sum_\mu \sin^2\left(\frac{p_\mu a}{2}\right) - i\sum_\mu \gamma_\mu \sin\left(p_\mu a\right)}{\left[\hat{m}_q + \frac{2r}{a}\sum_\mu \sin^2\left(\frac{p_\mu a}{2}\right)\right]^2 + \sum_\mu \sin^2\left(p_\mu a\right)} \\ &= \frac{\hat{M}(p) - i\sum_\mu \gamma_\mu \sin\left(p_\mu a\right)}{\hat{M}^2(p) + \sum_\mu \sin^2\left(p_\mu a\right)},\end{aligned}$$

where we defined $\hat{M}(p) \equiv \hat{m}_q + \frac{2r}{a}\sum_\mu \sin^2\left(\frac{p_\mu a}{2}\right)$.
For every $\hat{p}_\mu \neq (\pm\pi/a, \pm\pi/a)$, one has that $a \to 0$ implies $\hat{M}(p) \to \hat{m}_q$.
Instead, for every momentum vector that lies at the edge of the Brillouin zone $M(p) \to \infty$ as $a \to 0$. This removes the fermion doublers in the continuum limit.

A notable problem is that one then loses chiral symmetry since the Wilson term is clearly not invariant under neither the continuous transformation

$$\psi \to e^{i\theta\gamma_5}\psi \qquad \bar{\psi} \to -\bar{\psi}\, e^{i\theta\gamma_5},$$

nor the discrete

$$\psi \to \gamma_5 \psi \qquad \bar{\psi} \to -\bar{\psi}\gamma_5.$$

It is in fact proven that one either comepletely removes the doublers or breaks chiral symmetry [26].

Appendix C

Algorithms and technical details

cite also felipe for bilinear
In this basis

$$\frac{1}{2}\Gamma_{+\hat{0}} = \frac{1+\gamma_0}{2} = \begin{pmatrix} 1 & 0 \\ 0 & 0 \end{pmatrix} \qquad \frac{1}{2}\Gamma_{-\hat{0}} = \frac{1-\gamma_0}{2} \qquad = \begin{pmatrix} 0 & 1 \\ 0 & 0 \end{pmatrix}$$
$$\frac{1}{2}\Gamma_{+\hat{1}} = \frac{1+\gamma_1}{2} = \begin{pmatrix} 1 & 1 \\ 1 & 1 \end{pmatrix} \qquad \frac{1}{2}\Gamma_{-\hat{1}} = \frac{1-\gamma_1}{2} \quad = \begin{pmatrix} 1 & -1 \\ -1 & 1 \end{pmatrix}$$

$$(1-\gamma_0)\,\psi = \begin{bmatrix} 0 & 0 \\ 0 & 2 \end{bmatrix} \begin{bmatrix} \psi_1 \\ \psi_2 \end{bmatrix} = \begin{bmatrix} 0 \\ 2\psi_2 \end{bmatrix},$$
$$(1+\gamma_0)\,\psi = \begin{bmatrix} 2 & 0 \\ 0 & 0 \end{bmatrix} \begin{bmatrix} \psi_1 \\ \psi_2 \end{bmatrix} = \begin{bmatrix} 2\psi_1 \\ 0 \end{bmatrix},$$
$$(1-\gamma_1)\,\psi = \begin{bmatrix} 1 & -1 \\ -1 & 1 \end{bmatrix} \begin{bmatrix} \psi_1 \\ \psi_2 \end{bmatrix} = \begin{bmatrix} \psi_1 - \psi_2 \\ -\psi_1 + \psi_2 \end{bmatrix} \equiv \begin{bmatrix} \eta_{+1} \\ -\eta_{+1} \end{bmatrix},$$
$$(1+\gamma_1)\,\psi = \begin{bmatrix} 1 & 1 \\ 1 & 1 \end{bmatrix} \begin{bmatrix} \psi_1 \\ \psi_2 \end{bmatrix} = \begin{bmatrix} \psi_1 + \psi_2 \\ \psi_1 + \psi_2 \end{bmatrix} \equiv \begin{bmatrix} \eta_{-1} \\ \eta_{-1} \end{bmatrix}.$$

C.1 Conjugate Gradient algorithm and the Dirac operator

The full inversion of the Dirac operator is a very expensive computation, given that the Dirac operator has dimension $(2\,N_t\,N_x\,N_f)^2$, even though it is very sparse and has only few non-zero entries. One can note that for the purpose of computing the fermionic contribution to the drift force and the extraction of the physical quark mass from the correlator (details in section x and section y), only the inverse operator applied to a vector is needed. Hence it is sufficient to compute

$$\psi = D^{-1}\,|\eta\rangle \tag{C.1}$$

Computing ψ via equation (C.1) is equivalent to solve the linear system $D\psi = \eta$, which can be done efficiently by employing a method for sparse matrices such as Conjugate Gradient (CG) as explained in the following way.
We want to solve the equation

$$D\,\psi = \eta$$

CG requires the matrix to be hermitian while D is only γ^5-hermitian (really? under which assumptions?). One can thus solve the linear system

$$\left(DD^\dagger\right)\xi = \eta$$

and then obtain ψ by multiplying the solution ξ by $D^\dagger$ since

$$D^\dagger \xi = D^\dagger \left(DD^\dagger\right)^{-1} \eta = D^{-1}\eta = \psi \tag{C.2}$$

Analogously one can calculate

$$\chi = D^\dagger \eta$$

by solving

$$\left(D^\dagger D\right) \xi = \eta$$

and then applying D to the result.

C.2 Bilinear noise scheme

$$\mathrm{Tr}\left[D^{-1}\frac{\delta D}{\delta \phi^j}\right] \approx \langle \eta | D^{-1} \frac{\delta D}{\delta \phi^j} |\eta\rangle = \langle \psi | \frac{\delta D}{\delta \phi^j} |\eta\rangle \qquad |\psi\rangle = D^{-1}|\eta\rangle = D^\dagger \underbrace{(DD^\dagger)^{-1}|\eta\rangle}_{\text{CG}}$$

$$\mathrm{Tr}\ A = \frac{1}{N} \lim_{N\to\infty} \sum_i^N \eta_i^T D_{ij} \eta_j \tag{C.3}$$

where η_i is a gaussian random field where each component is drawn from a normal distribution $\mathcal{N}(0,1)$.
More precisely each vector component η_i^α satisfies

$$\langle \eta_i^\alpha \rangle = 0 \qquad \left\langle \eta_i^\alpha \eta_j^\beta \right\rangle = \delta_{i,j}\, \delta^{\alpha\beta}$$

The series (C.3) requires in principle an infinite number of vectors to evaluate the trace exactly. In practice we truncate it and choose $N = 1$:D :D. The average over Monte Carlo samples will eventually converge nevertheless to the right result.

Bibliography

[1] Istvan Montvay and Gernot Münster. *Quantum Fields on a Lattice*. 1994. DOI: 10.1017/cbo9780511470783.

[2] Heinz J Rothe. *Lattice Gauge Theories*. 4th. WORLD SCIENTIFIC, 2012. DOI: 10.1142/8229. URL: https://www.worldscientific.com/doi/abs/10.1142/8229.

[3] Christof Gattringer and Christian B. Lang. *Lattice quantum chromodynamics*. DOI: 10.1036/1097-8542.yb100080. URL: https://doi.org/10.1036%2F1097-8542.yb100080.

[4] Michael Creutz. *Quarks, Gluons and Lattices*. Cambridge Monographs on Mathematical Physics. Cambridge University Press, 2023. DOI: 10.1017/9781009290395.

[5] Y. Nambu and G. Jona-Lasinio. "Dynamical model of elementary particles based on an analogy with superconductivity. i". In: *Physical Review* 122.1 (1961). ISSN: 0031899X. DOI: 10.1103/PhysRev.122.345.

[6] Y. Nambu and G. Jona-Lasinio. "Dynamical model of elementary particles based on an analogy with superconductivity. II". In: *Physical Review* 124.1 (1961). ISSN: 0031899X. DOI: 10.1103/PhysRev.124.246.

[7] Andrea Carosso. *Novel Approaches to Renormalization Group Transformations in the Continuum and on the Lattice*. 2020. arXiv: 2006.07481 [hep-lat].

[8] L. D. Landau. "On the theory of phase transitions". In: *Zh. Eksp. Teor. Fiz.* 7 (1937). Ed. by D. ter Haar, pp. 19–32. DOI: 10.1016/B978-0-08-010586-4.50034-1.

[9] Vitaly L. Ginzburg. "On Superconductivity and Superfluidity (What I Have and Have Not Managed to Do), as well as on the 'Physical Minimum' at the Beginning of the 21st Century". In: *ChemPhysChem* 5.7 (2004), pp. 930–945. DOI: https://doi.org/10.1002/cphc.200400182. eprint: https://chemistry-europe.onlinelibrary.wiley.com/doi/pdf/10.1002/cphc.200400182. URL: https://chemistry-europe.onlinelibrary.wiley.com/doi/abs/10.1002/cphc.200400182.

[10] Tian Yu Cao, ed. *Conceptual foundations of quantum field theory. Proceedings, Symposium and Workshop, Boston, USA, March 1-3, 1996*. Cambridge, UK: CUP, 1999.

[11] Leo P. Kadanoff. "Scaling laws for ising models near T_c". In: *Physics Physique Fizika* 2 (6 June 1966), pp. 263–272. DOI: 10.1103/PhysicsPhysiqueFizika.2.263. URL: https://link.aps.org/doi/10.1103/PhysicsPhysiqueFizika.2.263.

[12] Kenneth G. Wilson. "Renormalization Group and Critical Phenomena. I. Renormalization Group and the Kadanoff Scaling Picture". In: *Phys. Rev. B* 4 (9 Nov. 1971), pp. 3174–3183. DOI: 10.1103/PhysRevB.4.3174. URL: https://link.aps.org/doi/10.1103/PhysRevB.4.3174.

[13] Kenneth G. Wilson. "Renormalization Group and Critical Phenomena. II. Phase-Space Cell Analysis of Critical Behavior". In: *Phys. Rev. B* 4 (9 Nov. 1971), pp. 3184–3205. DOI: 10.1103/PhysRevB.4.3184. URL: https://link.aps.org/doi/10.1103/PhysRevB.4.3184.

[14] Kenneth G. Wilson and Michael E. Fisher. "Critical Exponents in 3.99 Dimensions". In: *Phys. Rev. Lett.* 28 (4 Jan. 1972), pp. 240–243. DOI: 10.1103/PhysRevLett.28.240. URL: https://link.aps.org/doi/10.1103/PhysRevLett.28.240.

[15] John Cardy. "The renormalization group idea". In: *Scaling and Renormalization in Statistical Physics*. Cambridge Lecture Notes in Physics. Cambridge University Press, 1996, pp. 28–60. DOI: 10.1017/CBO9781316036440.004.

[16] Michael E. Peskin and Daniel V. Schroeder. *An Introduction to quantum field theory*. Reading, USA: Addison-Wesley, 1995. ISBN: 978-0-201-50397-5.

[17] Kenneth G. Wilson and J. Kogut. "The renormalization group and the ϵ expansion". In: *Physics Reports* 12.2 (1974), pp. 75–199. ISSN: 0370-1573. DOI: https://doi.org/10.1016/0370-1573(74)90023-4. URL: https://www.sciencedirect.com/science/article/pii/0370157374900234.

[18] Michel Le Bellac. *Thermal Field Theory*. Cambridge Monographs on Mathematical Physics. Cambridge University Press, 1996. DOI: 10.1017/CBO9780511721700.

[19] Erhard Seiler. "The case against asymptotic freedom". Applications of RG Methods in Mathematical Sciences. 2003.

[20] Sacha Friedli and Yvan Velenik. *Statistical Mechanics of Lattice Systems: A Concrete Mathematical Introduction*. Cambridge University Press, 2017. DOI: 10.1017/9781316882603.

[21] G. Parisi and Y.-S. Wu. "Perturbation Theory without Gauge Fixing". In: *Scientia Sinica* (24 1981), p. 483.

[22] Poul H. Damgaard and Helmuth Hüffel. "Stochastic quantization". In: *Physics Reports* 152.5-6 (Aug. 1987), pp. 227–398. ISSN: 0370-1573. DOI: 10.1016/0370-1573(87)90144-X.

[23] Crispin Gardiner. *Stochastic Methods: A Handbook for the Natural and Social Sciences*. Springer Berlin, Heidelberg, 2009, pp. XVIII, 447.

[24] Jan M. Pawlowski, Ion Olimpiu Stamatescu, and Felix P.G. Ziegler. "Cooling stochastic quantization with colored noise". In: *Physical Review D* 96.11 (2017). ISSN: 24700029. DOI: 10.1103/PhysRevD.96.114505.

[25] Matthew Schwartz. *Quantum Field Theory and the Standard Model*. Ed. by Cambridge: Cambridge University Press. 2013. DOI: doi:10.1017/9781139540940.

[26] H.B. Nielsen and M. Ninomiya. "Absence of neutrinos on a lattice: (I). Proof by homotopy theory". In: *Nuclear Physics B* 185.1 (1981), pp. 20–40. ISSN: 0550-3213. DOI: https://doi.org/10.1016/0550-3213(81)90361-8. URL: https://www.sciencedirect.com/science/article/pii/0550321381903618.

[27] Alejandro Ayala et al. *QCD phase diagram in a magnetized medium from the chiral symmetry perspective: the linear sigma model with quarks and the Nambu–Jona-Lasinio model effective descriptions*. 2021. DOI: 10.1140/epja/s10050-021-00534-4.

[28] Aneesh Manohar and Howard Georgi. "Chiral quarks and the non-relativistic quark model". In: *Nuclear Physics B* 234.1 (1984), pp. 189–212. ISSN: 0550-3213. DOI: https://doi.org/10.1016/0550-3213(84)90231-1. URL: https://www.sciencedirect.com/science/article/pii/0550321384902311.

[29] Kenneth G. Wilson. "Confinement of quarks". In: *Phys. Rev. D* 10 (8 Oct. 1974), pp. 2445–2459. DOI: 10.1103/PhysRevD.10.2445. URL: https://link.aps.org/doi/10.1103/PhysRevD.10.2445.

[30] G. G. Batrouni et al. "Langevin simulations of lattice field theories". In: *Phys. Rev. D* 32 (10 Nov. 1985), pp. 2736–2747. DOI: 10.1103/PhysRevD.32.2736. URL: https://link.aps.org/doi/10.1103/PhysRevD.32.2736.

[31] Andreas S. Kronfeld. "Dynamics of Langevin simulations". In: *Prog. Theor. Phys. Suppl.* 111 (1993), pp. 293–312. DOI: 10.1143/PTPS.111.293. arXiv: hep-lat/9205008.

[32] Virginia Vassilevska Williams et al. *New Bounds for Matrix Multiplication: from Alpha to Omega*. 2023. arXiv: 2307.07970 [cs.DS].

[33] Haim Avron and Sivan Toledo. "Randomized Algorithms for Estimating the Trace of an Implicit Symmetric Positive Semi-Definite Matrix". In: *J. ACM* 58.2 (Apr. 2011). ISSN: 0004-5411. DOI: 10.1145/1944345.1944349. URL: https://doi.org/10.1145/1944345.1944349.

[34] Werner Horsthemke. "Noise Induced Transitions". In: *Non-Equilibrium Dynamics in Chemical Systems*. Ed. by Christian Vidal and Adolphe Pacault. Berlin, Heidelberg: Springer Berlin Heidelberg, 1984, pp. 150–160. ISBN: 978-3-642-70196-2.

[35] Raúl Toral. "Noise-induced transitions vs. noise-induced phase transitions". In: *AIP Conference Proceedings* 1332.1 (Mar. 2011), pp. 145–154. ISSN: 0094-243X. DOI: 10.1063/1.3569493. eprint: https://pubs.aip.org/aip/acp/article-pdf/1332/1/145/12109027/145_1_online.pdf. URL: https://doi.org/10.1063/1.3569493.

[36] Felipe Attanasio, Jan Philipp Klinger, and Jan M. Pawlowski. *Low energy effective theories on the lattice with coloured noise*. 2022. arXiv: 2212.12354 [hep-lat].

[37] Yousef Saad. *Iterative Methods for Sparse Linear Systems*. Second. Society for Industrial and Applied Mathematics, 2003. DOI: 10.1137/1.9780898718003. eprint: https://epubs.siam.org/doi/pdf/10.1137/1.9780898718003. URL: https://epubs.siam.org/doi/abs/10.1137/1.9780898718003.

[38] Jeffrey Goldstone, Abdus Salam, and Steven Weinberg. "Broken Symmetries". In: *Phys. Rev.* 127 (3 Aug. 1962), pp. 965–970. DOI: 10.1103/PhysRev.127.965. URL: https://link.aps.org/doi/10.1103/PhysRev.127.965.

[39] Y. Iwasaki. "Phase diagram of QCD at finite temperatures with Wilson fermions". In: *Nucl. Phys. B Proc. Suppl.* 42 (1995), pp. 96–102. DOI: 10.1016/0920-5632(95)00191-B. arXiv: hep-lat/9412103.

[40] L. Maiani and G. Martinelli. "Current algebra and quark masses from a Monte Carlo simulation with Wilson fermions". In: *Physics Letters B* 178.2 (1986), pp. 265–271. ISSN: 0370-2693. DOI: https://doi.org/10.1016/0370-2693(86)91508-X. URL: https://www.sciencedirect.com/science/article/pii/037026938691508X.

List of Abbreviations

RG	**R**enormalisation **G**group
fRG	**F**unctional **R**enormalisation **G**group
UV	**U**ltra**v**iolet
QFT	**Q**uantum **F**ield **Theory**

Physical Constants

Speed of Light $c_0 = 2.997\,924\,58 \times 10^8\,\mathrm{m\,s^{-1}}$ (exact)

List of Symbols